Ocean Modelling 110 (2017) 66–82

Contents lists available at ScienceDirect

Ocean Modelling

journal homepage: www.elsevier.com/locate/ocemod

Virtual Special Issue
Coastal ocean modelling

A coupled wave-hydrodynamic model of an atoll with high friction: Mechanisms for flow, connectivity, and ecological implications

Justin S. Rogers[a,*], Stephen G. Monismith[a], Oliver B. Fringer[a], David A. Koweek[b], Robert B. Dunbar[b]

[a] Environmental Fluid Mechanics Laboratory, Stanford University, 473 Via Ortega, Y2E2 Rm 126, Stanford, CA, 94305, USA
[b] Department of Earth System Science, Stanford University, Stanford, CA, 94305, USA

ARTICLE INFO

Article history:
Received 18 April 2016
Revised 11 October 2016
Accepted 28 December 2016
Available online 29 December 2016

Keywords:
Coral reefs
Hydrodynamics
Surface water waves
Temperature, Atolls

ABSTRACT

We present a hydrodynamic analysis of an atoll system from modeling simulations using a coupled wave and three-dimensional hydrodynamic model (COAWST) applied to Palmyra Atoll in the Central Pacific. This is the first time the vortex force formalism has been applied in a highly frictional reef environment. The model results agree well with field observations considering the model complexity in terms of bathymetry, bottom roughness, and forcing (waves, wind, metrological, tides, regional boundary conditions), and open boundary conditions. At the atoll scale, strong regional flows create flow separation and a well-defined wake, similar to 2D flow past a cylinder. Circulation within the atoll is typically forced by waves and tides, with strong waves from the north driving flow from north to south across the atoll, and from east to west through the lagoon system. Bottom stress is significant for depths less than about 60 m, and in addition to the model bathymetry, is important for correct representation of flow in the model. Connectivity within the atoll system shows that the general trends follow the mean flow paths. However, some connectivity exists between all regions of the atoll system due to nonlinear processes such as eddies and tidal phasing. Moderate wave stress, short travel time (days since entering the reef system), and low temperature appear to be the most ideal conditions for high coral cover at this site.

1. Introduction

Coral reefs provide a wide and varied habitat that supports some of the most diverse assemblages of living organisms found anywhere on earth (Darwin, 1842). Coral reefs are critically important for the hundreds of millions of people reliant on them for food, storm protection, and cultural importance (Burke et al., 2011); yet they are under increased threat from climate change, ocean acidification and a host of local stressors (Hoegh-Guldberg et al., 2007; Hughes et al., 2003; Kleypas, 1999). Hydrodynamic flows influence the biological processes of coral reefs in several ways (Chappell, 1980) and therefore understanding their characteristics in reef environments is increasingly important (Monismith, 2007).

Hydrodynamic flows are the primary mechanism for dispersal and thus connectivity for small larval species such as corals (Cowen and Sponaugle, 2009) and connectivity between reef systems at inter-island scales using hydrodynamic models has been the subject of several studies (Andréfouët et al., 2002; Jones et al., 2009; Roberts, 1997). At smaller scales, atolls represent a geologic end ecologic member for reefs, and are common throughout the world's tropical oceans (Riegl and Dodge, 2008). The distinctive geometry of exterior reefs and interior lagoon system separated by a reef crest and reef flat with connecting channel systems is a unique feature which creates different interconnected hydrodynamic regimes. Previous studies on atolls have focused on portions of the system (Andréfouët et al., 2012, 2006; Dumas et al., 2012; Kench, 1998), but to our knowledge, no studies exist studying interconnectivity within an atoll system.

Reefs are areas of high productivity because they are efficient at trapping and recycling nutrients, thereby supporting both phytoplankton and zooplankton (Odum and Odum, 1955; Yahel et al., 1998). Water motion appears to be beneficial to coral reefs through increasing the rates of nutrient uptake, photosynthetic production and particulate capture (Atkinson and Bilger, 1992; Carpenter et al., 1991; Genin et al., 2009). Reef-building corals

* Corresponding author.
E-mail address: jsrogers@stanford.edu (J.S. Rogers).

http://dx.doi.org/10.1016/j.ocemod.2016.12.012
1463-5003/

have experienced global declines resulting from bleaching events caused week to month-long warm-water exposure (Carpenter et al., 2008; Hoegh-Guldberg et al., 2007; Hughes et al., 2003). However, corals in naturally warm environments can exhibit enhanced resistance to bleaching at high temperatures through both short-term acclimatory and longer-term adaptive acquisition of climate resistance (Palumbi et al., 2014). Terrestrial systems often negatively impact reefs through increased nutrient loading and sedimentation, among other factors (Acevedo et al., 1989; Buddemeier and Hopley, 1988; Fabricius, 2005; Rogers, 1990); and the retention and removal of terrigenous sediment depends on hydrodynamic processes (flushing rates, dilution), hydrology (e.g., accumulation and groundwater discharge) as well as biological processes (Fabricius, 2005).

The hydrodynamics of reef systems are governed primarily by the forcing mechanisms that drive flow, typically waves, tides, regional flow, wind, and buoyancy effects. These mechanisms have different importance depending on the scale (Monismith, 2007). At the island scale, typically kilometers, the flow is primarily governed by the interaction of the island with the large-scale regional flow, tides, Coriolis effects, and buoyancy (Monismith, 2007). Depending on flow conditions, vortices can be shed from local bathymetric features such as headlands, or from the island itself (Arístegui et al., 1994; Wolanski et al., 1996).

At the reef scale, typically ten to hundreds of meters, waves have long been recognized as the dominant forcing mechanism on many reefs (Callaghan et al., 2006; Kraines et al., 1998; Lowe et al., 2009a; Lugo-Fernández et al., 2004; Munk and Sargent, 1954; Symonds et al., 1995). Conceptually, wave dissipation from breaking or bottom friction increases the mean water level, known as wave setup, establishing a pressure gradient that drives flow across the reef in the direction of wave propagation (Lowe et al., 2009b; Munk and Sargent, 1954; Young, 1989). In addition, tides can play a more direct role in driving circulation in larger and more enclosed lagoons where the channels connecting the lagoon with the open ocean are relatively narrow, and the constricted exchange of water between these lagoons and the open ocean can cause significant phase lags between lagoon and offshore water levels (e.g., Dumas et al., 2012; Lowe and Falter, 2015). Wind stresses often play only a minor role in driving the circulation of shallow reefs; however, wind forcing can be important or even dominant in the circulation of deeper and more isolated lagoons (Atkinson et al., 1981; Delesalle and Sournia, 1992; Douillet et al., 2001; Lowe et al., 2009a). Finally, buoyancy forcing can drive reef circulation through either temperature- or salinity-driven stratification, which may also be important in certain reef systems (Hoeke et al., 2013; Monismith et al., 2006).

The classical dynamical basis by which waves drive flow is by changes to the waves from physical processes such as shoaling, refraction, dissipation, etc., which create spatial gradients in radiation stresses and impart a force in the momentum equation (Longuet-Higgins and Stewart, 1964). The radiation stress gradient can be recast as a vortex force in the full three-dimensional momentum equations, first proposed by Craik and Leibovich (1976) and developed more fully by Uchiyama et al. (2010). The vortex force is the interaction of the Stokes drift with flow vorticity, and is essential in the mechanism for Langmuir circulation. The vortex force formalism has recently been implemented in numerical models, and has shown increased skill over traditional radiation stress methods in predicting velocity profiles in conditions of coincident waves and currents (Kumar et al., 2015, 2012). While the vortex force formalism has shown good results in certain field conditions, it has not yet been implemented on coral reefs with high bottom drag and steep slopes.

Corals have irregular, branching morphologies and reef topography varies at scales ranging from centimeters to kilometers, therefore flow within these systems is complex (Rosman and Hench, 2011). In circulation models, variability in reef geometry occurs at scales smaller than the resolution of the computational grid; thus, drag due to the small scale geometry must be parameterized. On reefs, bottom friction is often a significant term in the momentum balance and the primary dissipation loss; and thus correct parameterization of the bottom drag is essential (Monismith, 2007).

Understanding the hydrodynamics across a range of spatial and temporal scales is necessary for understanding coral reef ecosystem function since critical ecosystem processes such as larval dispersal, and hence genetic connectivity, are heavily dependent upon atoll hydrodynamics. Thus the potential of coral reefs to withstand a warmer and more acidic future is partly informed by better understanding the hydrodynamics of atoll-wide coral reef ecosystems. The goals of this study were to apply a hydrodynamic model using the vortex force implementation in a high frictional reef environment and validated through extensive field observations to better understand the processes, timescales, and spatial scales that govern the hydrodynamics and connectivity on a model atoll. We first assess the performance of the hydrodynamic model and examine the effects of different forcing mechanisms in driving flow at the scale of the atoll itself, as well as circulation within the atoll system. We then investigate the interconnectivity of the atoll and address the role of hydrodynamics in shaping its ecological community structure.

2. Methods and study site

2.1. Field study site and observations

Numerous small islands and atolls dot the Central Pacific, including Palmyra Atoll, in the Northern Line Islands. The Northern Line Islands in the central equatorial Pacific are of significant ecological interest (Sandin et al., 2008; Stevenson et al., 2007). Palmyra Atoll in particular because of its status as a National Wildlife Refuge (5° 52′N, 162° 05′W) (Fig. 1a,b), is thought to represent a reef with little anthropogenic degradation and abundant calcifiers. Palmyra's exposed reef tracts (outside of the lagoons) contain abundant and diverse calcifiers, namely hard corals and crustose coralline algae (Williams et al., 2013) with relatively high community production and calcification rates (Koweek et al., 2015b). Thus, characterizing the hydrodynamics in this isolated atoll system with an intact exterior reef structure and highly frictional environment is of interest (Monismith et al., 2015; Rogers, 2015; Rogers et al., 2016a, 2016b, 2015).

The atoll consists of a forereef, reef crest and shallow back reef region on both its northern and southern sides, while the western and eastern edges are dominated by open terraces of 5 to 20 m depth with abundant corals (Fig. 1). The forereefs are characterized by high percentages of live stony coral cover (Fig. 1c,e), and typical spur and groove formations (Rogers et al., 2015). Near the reef crest where the surfzone is found, the substrate largely consists of rubble whereas further inshore, larger corals are common on the back reef. The open terraces are typically characterized by high live coral cover with high rugosity and complex bathymetry (Fig. 1d,e), while lagoonal areas typically exhibit soft sediment substrates (Williams et al., 2013).

Field observations of waves, currents, temperature were conducted on the atoll from 2012 to 2014 (Fig. 2) with additional details and results in Rogers (2015); Rogers et al. (2016a), and (2016b). The wave climate is seasonal, dominated by storm waves (1–3 m) from the north in the northern hemisphere winter, and storm waves (1–2 m) from the south in the southern hemisphere winter (Fig. 2a) (Rogers et al., 2016a). The tidal range is typically 0.8 m, with seasonal long-term sea level fluctuations of 0.2 m

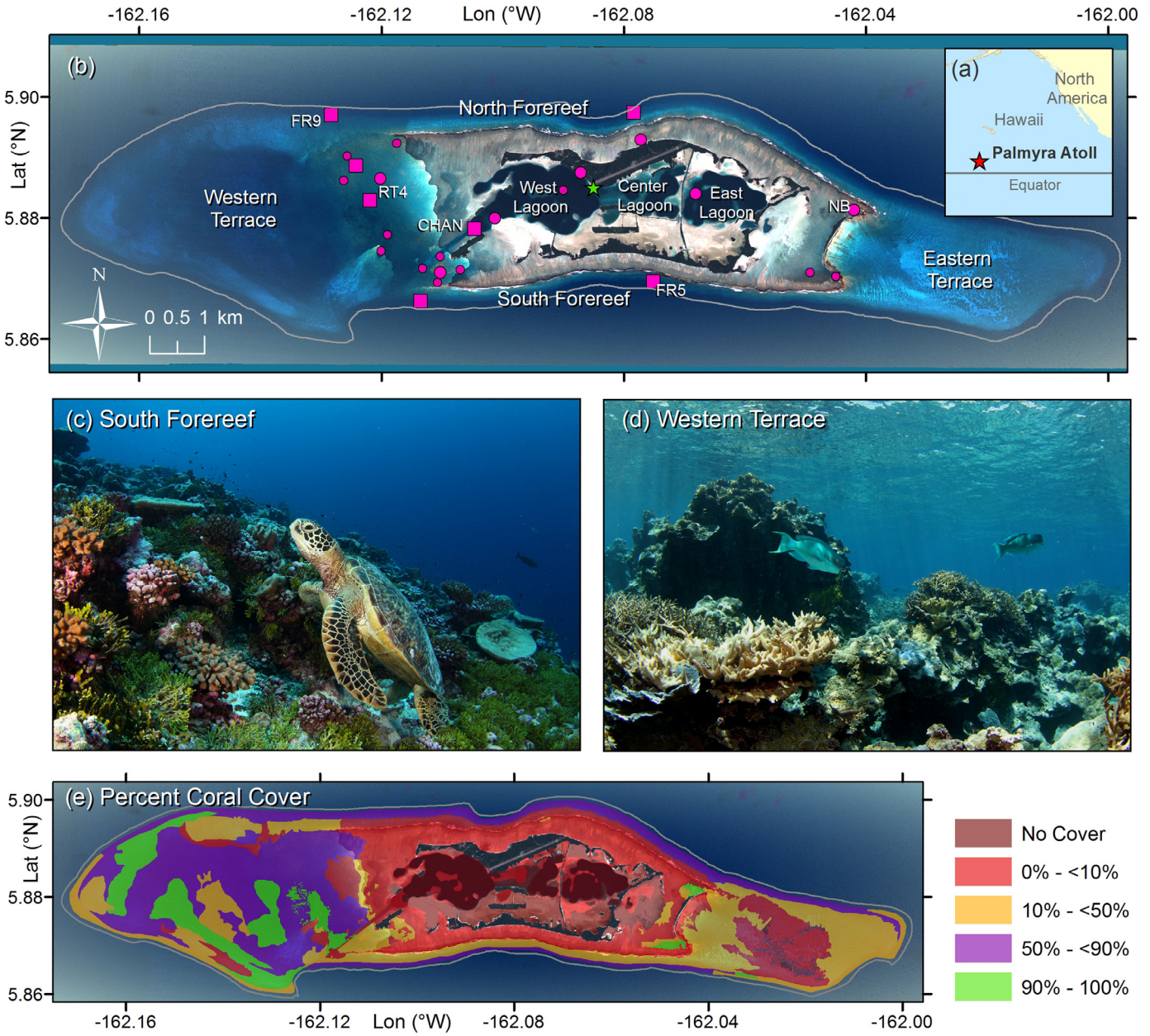

Fig. 1. Palmyra Atoll location, site layout and experiment instrumentation (a) location of Palmyra Atoll, (b) layout of atoll and instrument locations for long term measurement [(U, ζ, T) magenta squares; (ζ, T) magenta circles; (T) small magenta circles), and weather station (green star), image courtesy of NOAA. (c) typical southern forereef with abundant live coral and green sea turtle (*Chelonia mydas*), (d) typical rugose reef on shallow terrace with live coral and fish, and (e) percent coral cover mapping courtesy of NOAA. Gray line on (b, e) is 100 m depth contour, (c, d) courtesy of Brian Zgliczynski. (For interpretation of the references to colour in this figure legend, the reader is referred to the web version of this article.)

(Fig. 2b). The winds on the atoll are dominated by the northeasterly trade winds for much of the year, and are strongest in February through May, typically near 5 m/s (Fig. 2c) (Maragos et al., 2008; Rogers, 2015). The atoll is generally within the North Equatorial Counter Current (NECC), which flows primarily to the east at typically 0.2 to 0.8 m/s from August to January, and is weak the rest of the year (Fig. 2d) (Hsin and Qiu, 2012; Maragos et al., 2008), while large scale tropical instability waves are common in this region (Stevenson et al., 2015). Weekly average water temperatures on the atoll are typically 27 to 30 °C and vary seasonally, while 95% of local diurnal temperature fluctuations are typically within 1 °C of the mean (Fig. 2e) (Gardner et al., 2014b). Low pass filtering for these results and modeling results in the following sections was done using a spectral cutoff filter.

2.2. Coupled wave-hydrodynamic model

The Coupled-Ocean-Atmosphere-Wave-Sediment Transport (COAWST) program (Warner et al., 2010) was used to model the atoll. Only the ocean (Regional Ocean Modeling System – ROMS) and wave (Simulating Waves in the Nearshore – SWAN) modules were used in this study. The SWAN wave component of the model (Booij et al., 1999) contains a modified wave bottom friction formulation (Rogers et al., 2016a) to account for the very high wave friction factors from field observations (Monismith et al., 2015).

ROMS is a three-dimensional, free surface, topography following numerical model, which solves finite difference approximation of Reynolds Averaged Navier Stokes equations using hydrostatic and Boussinesq approximation with a split explicit time stepping

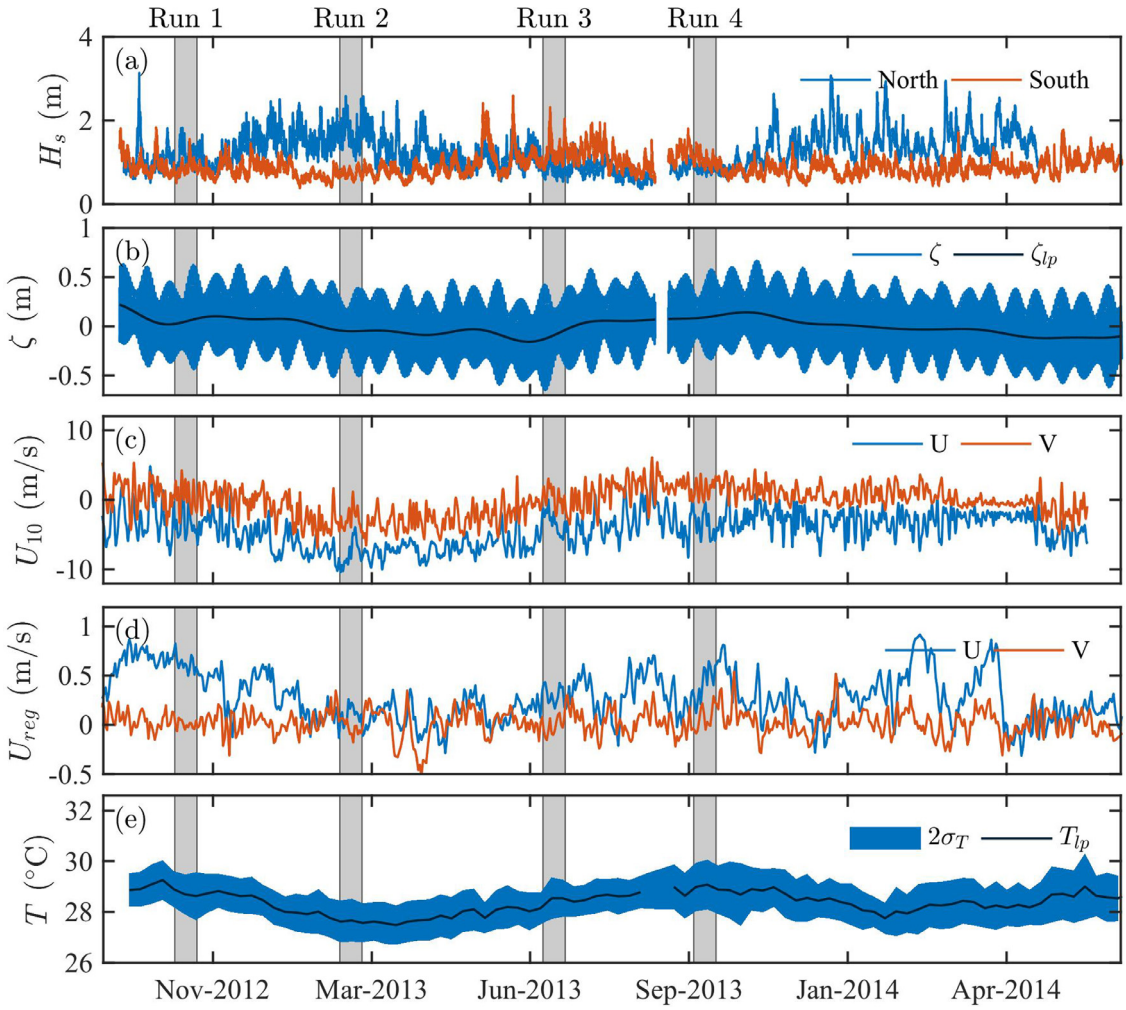

Fig. 2. Oceanographic setting and model forcing parameters from 2012 to 2014 during model run times for Runs 1 to 4. Forcing from (a) significant wave height H_s offshore of the northern and southern sides of the atoll, (b) free surface height ζ, (c) wind U_{10} (direction wind is going), (d) regional currents U_{reg} (avg. of upper 50 m of HYCOM) and (f) temperature T (avg. of all field records). Low pass filtering ($_{lp}$) is on a weekly average. Gray bars show extent of model runs.

algorithm (Haidvogel et al., 2008; Shchepetkin and McWilliams, 2009, 2005). The vortex force formalism expresses the Navier Stokes equations to include the effects of waves (Uchiyama et al., 2010),

$$\frac{\partial \boldsymbol{u}}{\partial t} + (\boldsymbol{u}\cdot\nabla_\perp)\boldsymbol{u} + w\frac{\partial \boldsymbol{u}}{\partial z} + f\hat{z}\times\boldsymbol{u} + \nabla_\perp\varphi - \boldsymbol{F} - \boldsymbol{D} + \frac{\partial}{\partial z}\left(\overline{u'w'} - \nu\frac{\partial \boldsymbol{u}}{\partial z}\right) = -\nabla_\perp\kappa + \boldsymbol{J} + \boldsymbol{F^w}, \quad (1)$$

where ($\boldsymbol{u}$, w) are the Eulerian mean velocities, z is the vertical coordinate, f is the Coriolis parameter, φ is the dynamic pressure (normalized by density), $\boldsymbol{F}$ is the non-wave, non-conservative force, $\boldsymbol{D}$ is the diffusive terms (viscosity and diffusion), ν is the molecular viscosity, κ is the lower order Bernoulli head, $\boldsymbol{F^w}$ is the sum of momentum flux due to all non-conservative wave forces, and $\boldsymbol{J}$ is the horizontal vortex force,

$$\boldsymbol{J} = -\hat{z}\times\boldsymbol{u^{st}}\left[\left(\hat{z}\cdot\nabla_\perp\times\boldsymbol{u}\right) + f\right] - w^{st}\frac{\partial \boldsymbol{u}}{\partial z}, \quad (2)$$

where ($\boldsymbol{u^{st}}$, w^{st}) is the Stokes drift.

The vortex force formalism is implemented in ROMS which solves for the Eulerian mean velocities and has shown improved skill in computed wave-driven velocities over the more traditional radiation stress gradient formulation (Kumar et al., 2012). The significant terms in the three dimensional momentum equation, are then acceleration (ACC), horizontal advection (HA), vertical advection (VA), Coriolis (COR), Stokes-Coriolis (StCOR), pressure gradient (PG), horizontal vortex force (HVF), non-wave body force (BF), wave breaking acceleration (BA), wave roller acceleration (RA), bottom streaming (BtSt), surface streaming (SuSt), horizontal mixing (HM), vertical mixing (VM), and curvilinear grid (FCurv). Vertical integration of the three dimensional equations, applying surface and bottom boundary conditions, assuming a rectangular grid, and ignoring wave streaming and Stokes-Coriolis effects gives the two-dimensional momentum equation (Kumar et al., 2012),

$$\mathrm{ACC} + \mathrm{HA} - \mathrm{COR} = -\mathrm{PG} + \mathrm{HVF} - \mathrm{Bstr} + \mathrm{Sstr} + [\mathrm{BA} + \mathrm{RA}] + \mathrm{HM}, \quad (3)$$

where bottom stress (Bstr) and surface stress (Sst) arise from the boundary conditions.

The model grid consists of a rectangular (x,y) grid covering 34.1 by 14.1 km at 50 m grid resolution, extending from −162.2387 to −161.9313 °W and 5.8189 to 5.9470 °N (Fig. 3a,b). Vertical resolution consists of 20 vertical layers in sigma-coordinates (3.8 M total grid cells). The data used for the model bathymetry is based on NOAA ship-based multi-beam bathymetry for depths greater than 10 m, and linear regression of 5 m grid IKONOS multispectral data for shallow depths [Pacific Islands Benthic Habitat Mapping Center, http://www.soest.hawaii.edu/pibhmc]. Grid bathymetry is interpolated from data sources and smoothed using a Shapiro

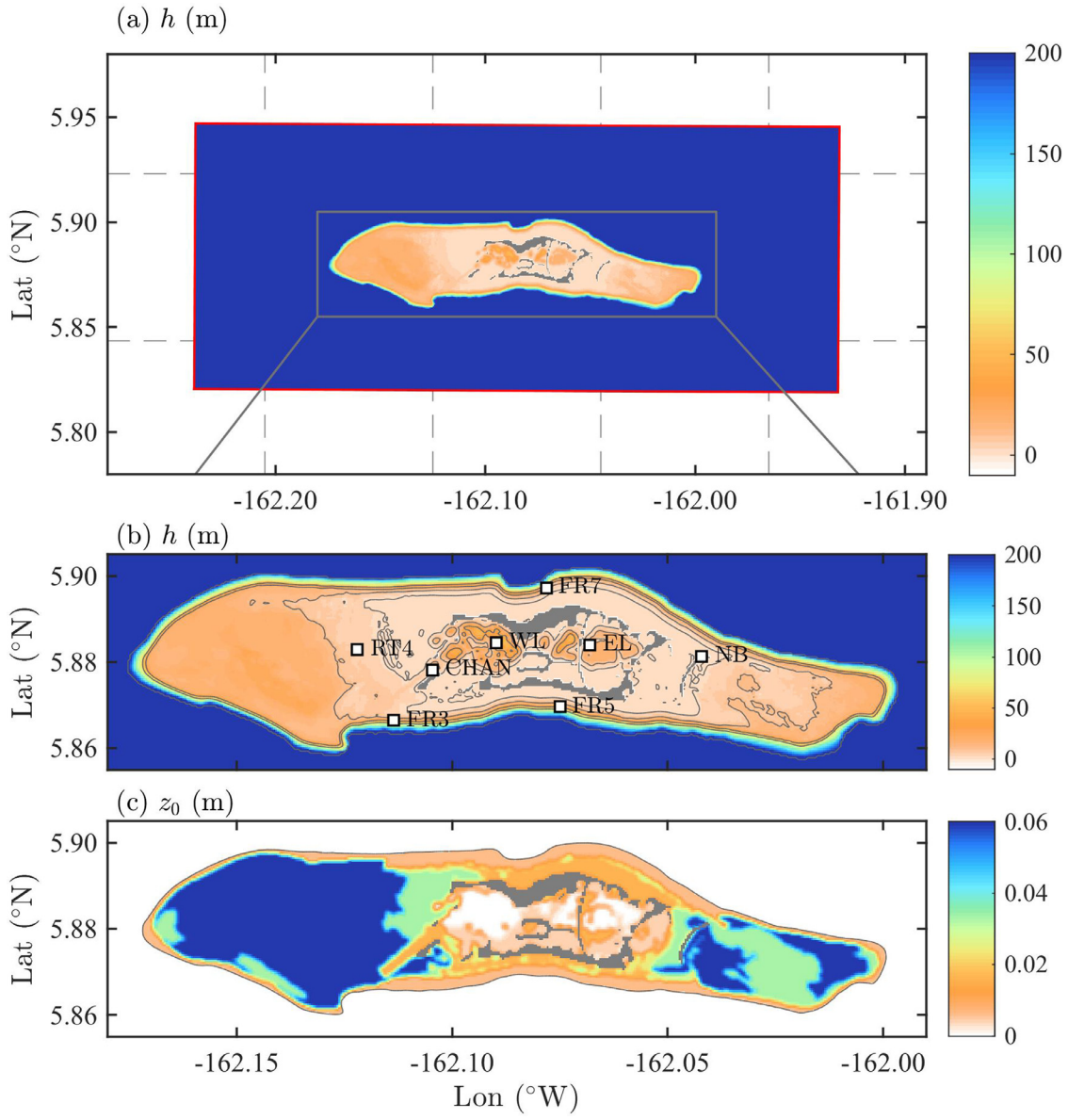

Fig. 3. Model grid layout, bathymetry and bottom roughness. (a) Model grid extent (red outline) and bathymetry, with HYCOM boundary condition grid (gray –), (b) depth grid detail h (m) zoomed to atoll with location of selected instrument stations, and (c) bottom roughness grid z_0 (m). Gray lines are (2, 10, 30, 60, 200 m) depth contours for (b), and 60 m for (c); gray shading is land mask. (For interpretation of the references to colour in this figure legend, the reader is referred to the web version of this article.)

filter until the appropriate grid stiffness parameters were met (Shchepetkin and McWilliams, 2003). A relatively small model domain is adequate for this setting because the atoll is isolated from other bathymetric features and the large scale flows generally exit the model domain. The reef crest is explicitly included in the grid based on field measurements and aerial images, and to reduce the complexity of the model, max depth was limited to 200 m, essentially the upper ocean mixed layer. Mapping of the dominant biological cover (Fig. 1e) was obtained from NOAA NCCOS Benthic Habitat Mapping (http://ccma.nos.noaa.gov/ecosystems/coralreef/palmyra), and in conjunction with computed values of bottom roughness heights z_0 across the atoll (Rogers, 2015) are used to infer a spatially variable z_0 over the model domain (Fig. 3c). A consistent grain size grid is input to both the ROMS and SWAN models. For the ROMS model, the Sherwood, Signell, Warner bottom boundary layer closure is employed to include both wave and mean current bottom stress (Warner et al., 2010). The SWAN wave model uses a revised friction formulation which correctly parameterizes the high wave friction on the atoll, as well as breaking coefficient values obtained from site data (Rogers et al., 2016a).

Initial conditions and lateral boundary conditions for velocity $\boldsymbol{u}$, temperature T, salinity S, and free surface height ζ, are interpolated from the National Ocean Partnership Program (NOPP)'s HYbrid Coordinate Ocean Model (HYCOM) global ocean model (http://hycom.org) (Fig. 3a). The ROMS open boundary conditions are Chapman for the free surface, Flather for 2D momentum, radiative with nudging for 3D momentum T, and S, and gradient for TKE similar to Kumar et al. (2015). Initial conditions for T and S within the lagoon system are taken from the WL temperature mooring observations, and annual CTD casts within the lagoon. In order that broad regional temperatures are similar between the model and field observations, the HYCOM initial (outside the lagoon interior) and boundary condition temperatures are adjusted by a spatially constant offset such that two-week average of the spatially averaged temperature of the upper 50 m depth from the HYCOM model match the two-week average of field observations on the atoll exterior forereefs. This is similar to

climatology routines employed in regional models, and offsets were typically less than a degree C. Tidal constituents are derived from the 2011 Oregon State University Pacific Ocean 1/12° Tidal Atlas (OTIS) (Egbert and Erofeeva, 2002). The generic length scale turbulence scheme is employed with coefficients consistent with the k-ε model (Warner et al., 2005).

Boundary conditions for the SWAN model are taken from measured wave height and period on the north (FR9) and south (FR5) of the atoll, corrected for changes to refraction, shoaling, and travel time from the measured location to the model boundary conditions, with wave angle taken from the NOAA Wave Watch III Hawaii Model results, and directional waves resolution is 5° (Rogers et al., 2016a).

Atmospheric winds, shortwave and longwave radiation, rainfall, air temperature, relative humidity, and air pressure were included in the model and taken from a weather station on the atoll (Fig. 1b) and implemented using the bulk fluxes model in ROMS. For periods of time when data was not available from on island measurements, atmospheric forcing was interpolated from NASA's Modern-Era Retrospective Analysis for Research and Applications (MERRA) global atmospheric model (http://disc.gsfc.nasa.gov). Notably, these periods include wind (prior to Sep-2013), rainfall (after Dec-2013), and longwave radiation (prior to Sep-2013).

Four separate periods of simulation were modeled using the COAWST model. Computations were run in parallel on 64 AMD Opteron (2.4 GHz) cores and due to processing time limitations, runs were limited to 14 day periods, which typically took 7500 cpu hours each. The first simulation, referred to as Run 1, simulates 3-Nov to 17-Nov 2012, and is a period of relatively average conditions with waves from the north (1.19 m H_s), eastern regional currents at 0.6 m/s, light winds, and average temperatures (Fig. 2). Runs 2 through 4 represent periods of variation in forcing parameters such as very strong northern waves (Run 2), strong southern waves (Run 3), weak waves (Run 4), weak regional flows (Run 2), and different direction of regional flow (Run 4) (Fig. 2).

The offshore travel time, or age represents the amount of time an individual fluid parcel or particle has spent inside of a domain since it entered a boundary (Monsen et al., 2002), here taken as the 100 m bathymetric depth contour. Lagrangian floats were released for each simulation starting approximately 2 days after model initialization, with some simulations varying this time to vary the tidal cycle of release. Here, Lagrangian refers to the floats with neutral density following the mean flows within the ROMS model, (which are essentially Eulerian) but do not include the effects of Stokes drift. This approximation may underestimate transport very near the surface when Stokes drift from waves is strong, but is likely reasonable otherwise. 22,447 floats were released within the model domain in and around the atoll, spaced evenly between the bottom, mid and top of the water column. Travel time was computed for each float as the time since the float crossed the 100 m bathymetric contour into the atoll. Results of travel time for all particle tracks were interpolated to a fine scale 10 m grid and then down sampled to the model grid using a median filter. Age is the converse of the commonly reported Lagrangian residence time, defined as a time taken for a parcel of fluid to leave a boundary (Monsen et al., 2002). For this system, travel time is a more relevant metric since we are most interested in how offshore waters are modified within the atoll system by interactions with organisms, terrestrial runoff, and the substrate.

3. Results

3.1. Model data comparison

Four separate periods of simulation (Runs 1 - 4) were modeled to characterize different forcing conditions. Run 1 is used for validation because it is the period of average conditions with substantial coincident field data (Fig. 2) (Rogers, 2015). The model results compare well to measured field observations for free surface height ζ, depth averaged alongshore flow U_{AS}, depth averaged cross-shore flow U_{CS}, and bottom temperature T_b at three selected sites, and for velocity and temperature in both 36-hour subtidal filtered ($\overline{U_{AS}}, \overline{U_{CS}}, \overline{T_b}$) and high frequency variability (U'_{AS}, U'_{CS}, T'_b) (Fig. 4). Additionally, the significant wave height has been previously shown to have good agreement between the model and field observations (Rogers et al., 2016a).

Table 1
Model skill compared to site observations for free surface height $\boldsymbol{\zeta}$, significant wave height $\boldsymbol{H_s}$, alongshore and cross-shore depth averaged velocity (U_{AS},U_{CS}), and near bottom temperature T_b, during Run 1 (Nov 2012).

Variable	Field Sites	Avg. Skill	Std. Skill
ζ	12	0.98	0.02
H_s	4	0.87	0.15
$\overline{U_{AS}}$	7	0.32	0.15
$\overline{U_{CS}}$	7	0.39	0.16
U'_{AS}	7	0.42	0.16
U'_{CS}	7	0.49	0.20
$\overline{T_b}$	23	0.73	0.17
T'_b	23	0.58	0.20

Note: skill excludes initial 3 days for model spin up, () is 36 h low pass filter, (′) is high pass, i.e. $T_b = \overline{T_b} + T'_b$.

To compare model predictions of a given variable of interest X_{model} to the observations X_{obs} in reef environments (Lowe et al., 2009a; Rogers et al., 2016a), we used a quantitative measure of model skill (Willmott, 1982),

$$\text{Skill} = 1 - \frac{\sum (X_{model} - X_{obs})^2}{\sum \left(\left| X_{model} - \overline{X_{obs}} \right| + \left| X_{obs} - \overline{X_{obs}} \right| \right)^2}, \quad (4)$$

where perfect agreement between model results and observations will yield a skill of one and complete disagreement yields a skill of zero. Over all available field data sites, average model skill for ζ is 0.98, for $\bar{U}$ is 0.36, for U' is 0.46, for $\overline{T_b}$ is 0.73 and T'_b is 0.58 (Table 1), with more detailed validation information in Rogers (2015) and Rogers et al. (2016a). Overall, after a period of about 2 days for model spin up, the COAWST model results for ζ, H_s, U_{AS}, U_{CS}, and T_b reasonably represent the mean and high frequency variability at each site in simulating the field scale flows observed on the atoll.

3.2. Tides

The open boundaries of the model are forced with tidal information from the OTIS database. On the atoll exterior forereefs and lagoon entrance channel, tidal amplitude is in excellent agreement and tidal phase is reasonably in agreement (Fig. 5). Within the innermost lagoon (East Lagoon), the model over predicts the tidal amplitude and under predicts the phase compared to the observations (Fig. 5). This discrepancy is likely due to inadequate resolution of the openings to the East Lagoon inlets which on the atoll vary from 10 to 100 m width whereas the grid scale is 50 m. Thus, the OTIS database does well represent the tidal fluctuations on the exterior of the atoll but the East Lagoon is more open to exchange in the model and tidal exchange is not sufficiently damped.

3.3. Vertical structure of velocity and temperature

The root mean square (rms) vertical velocity profiles on the forereef are reasonably predicted in the cross shore direction, while in the alongshore direction the general logarithmic profile shape is correct, and the model reasonably predicts the magnitude

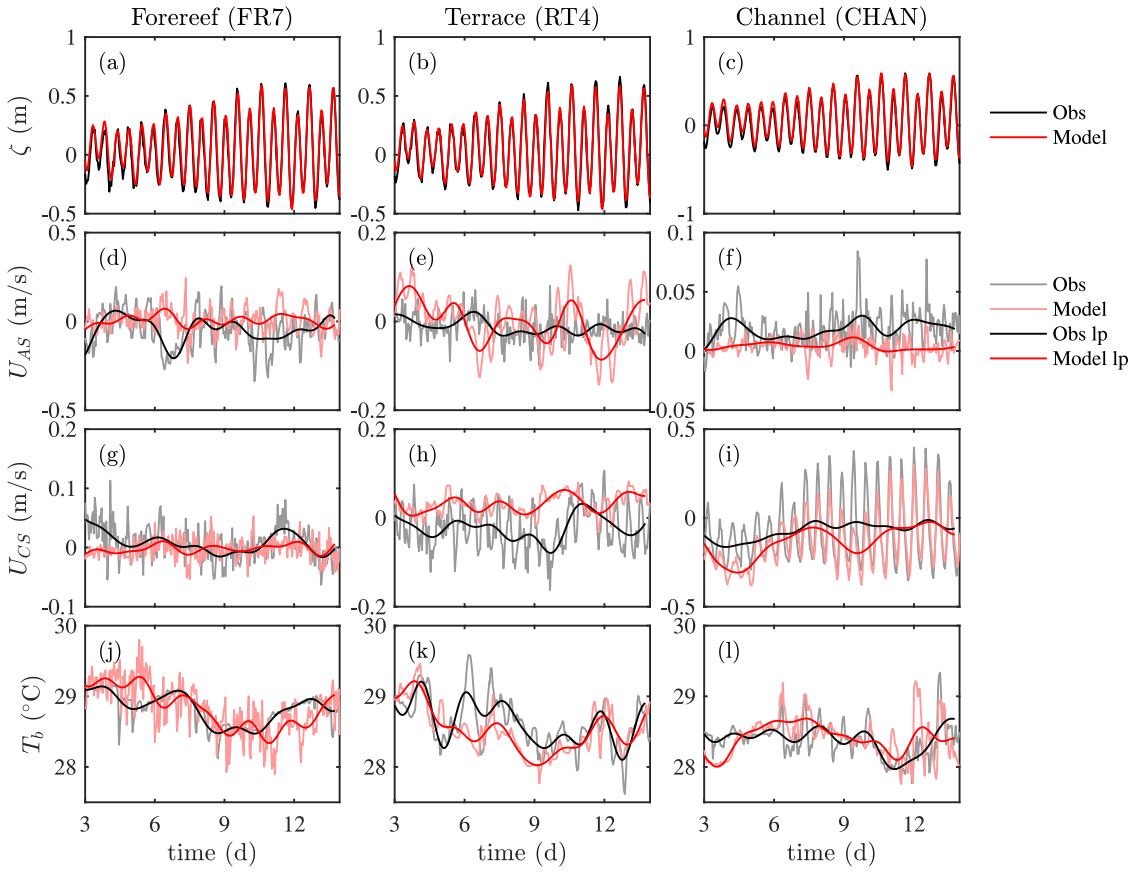

Fig. 4. Selected model validation data for three sites (FR7, RT4, and CHAN) for Run 1 (Nov-2012) for (a-c) mean surface height ζ, (d-f) depth averaged alongshore velocity U_{AS}, (g-i) depth averaged cross-shore velocity U_{CS}, and (j-l) near-bottom temperature T_b. Black is field observation, red is model result, for (d-l), light colors are instantaneous values and dark colors are subtidal filtered (36 hr). Time is since start of model run; three days of model spinup not shown. (For interpretation of the references to colour in this figure legend, the reader is referred to the web version of this article.)

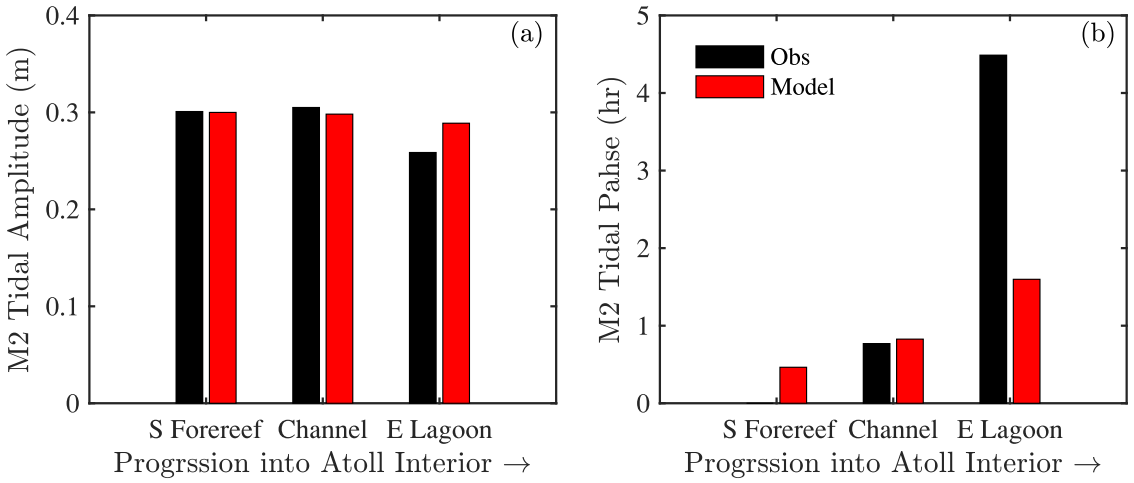

Fig. 5. Comparison of observed and modeled M2 tides. (a) tidal amplitude and (b) tidal phase for observations (black) and model (red) for Run 1 (Nov 2012), with progression into atoll interior at three sites (FR3, CHAN, EL). (For interpretation of the references to colour in this figure legend, the reader is referred to the web version of this article.)

(Fig. 6a,b). In the channel, both cross- and alongshore rms velocity profiles $\bar{u}_{rms}$, are in good agreement with field observations (Fig. 6c). The West Lagoon did not have field observations, but the model results show an rms profile consistent with wind driven surface shear (Fig. 6d).

The average temperature profiles $\bar{T}$, are in good agreement at the Forereef and Channel sites (Fig. 6e,f,g). In the West Lagoon, $\bar{T}$ is in good agreement in the upper 25 m mixed layer, but the model significantly over predicts $\bar{T}$ in the lower 25 m (Fig. 6h).

4. Discussion

4.1. Recipes for successful simulations in an atoll system

The model skill is excellent for the free surface and waves, and the model reasonably reproduces the mean and overall variability of velocities and temperature, which is typical of field scale models (Kumar et al., 2015). Differences in modeled and observed subtidal velocities on the forereef are likely influenced by the

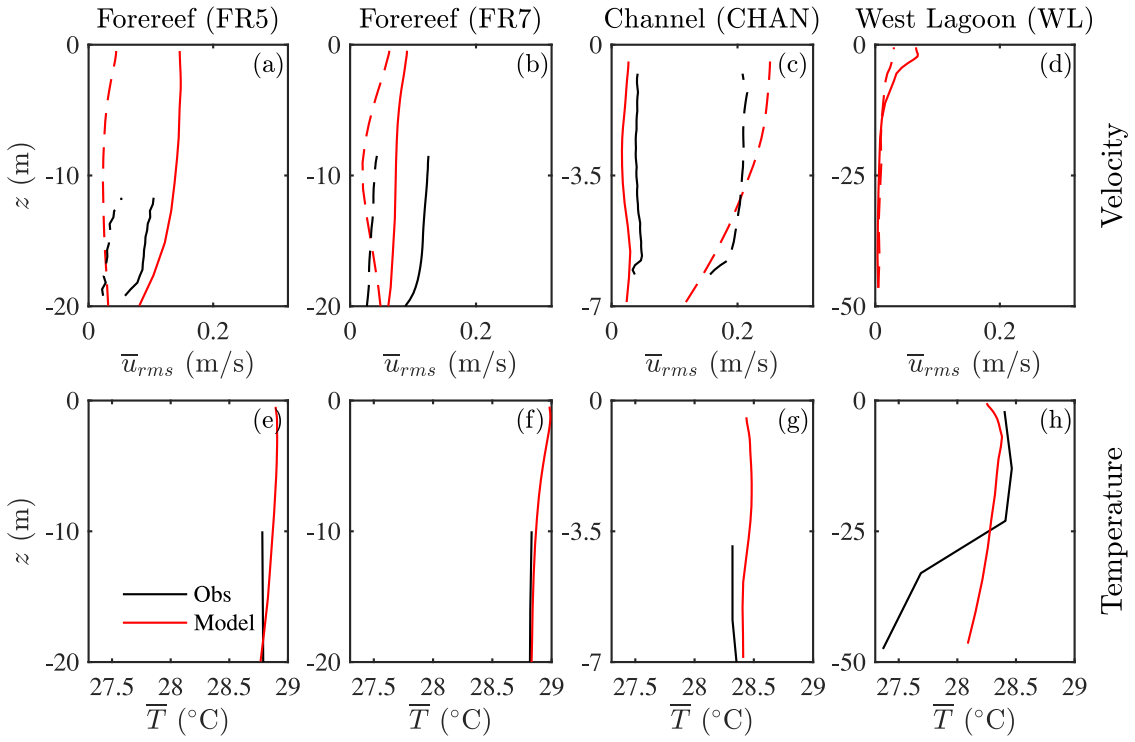

Fig. 6. Comparison of vertical profiles of velocity (top) and temperature (bottom) for observations (black) and model results (red) at four sites for Run 1 (Nov 2012). (a-d) root mean square (rms) velocity $\tilde{\boldsymbol{u}}_{\boldsymbol{rms}}$ in alongshore (-) and cross-shore (–) directions, and (e-h) average temperature $\bar{\boldsymbol{T}}$ profiles. Time averages exclude three days of model spin up. No field measurements available for (d). (For interpretation of the references to colour in this figure legend, the reader is referred to the web version of this article.)

incoming boundary conditions from the HYCOM model, which cannot explicitly model mesoscale and submesoscale eddies which are stochastic in nature. Considering the model complexity due to variable bathymetry and bottom roughness, multiple types of forcing (waves, wind, meteorological, tides, regional boundary conditions), and open boundary conditions from a global model, the results for depth averaged quantities, tides, and vertical structure are in good agreement with the field observations.

For predicting local flows on the atoll, bathymetry is a critical input parameter, especially in areas of strong hydrodynamic control such as the reef crest, channel, and lagoon inlets. Additionally, a critical factor is smoothing the grid sufficiently to achieve model stability, while still maintaining realistic geometry. Finally, because bottom stress is a significant term in the momentum balance for areas of shallow depth on the atoll, correct parameterization of bottom roughness is essential (Hench et al., 2008) and is achieved here through site observations of roughness and extended spatially through habitat mapping.

Areas of the model which are not well resolved due to the grid resolution include the East Lagoon inlets, which allow higher exchange through this lagoon in the model. This could be improved through higher grid resolution in these areas or parameterization of this subgridscale process such as weir flow or increased drag.

The average temperature profiles are in good agreement at the Forereef and Channel sites; the means are in agreement likely due to the offset adjustment of boundary condition temperatures from the HYCOM model. However, in the West Lagoon, the model significantly over predicts temperature in the lower 25 m. Since the model was initiated with realistic T and S profiles, the reason for this deviation is likely areas of too much mixing in the deep lagoon created by small $O(0.1$ cm/s) spurious vertical velocities along the sides of the lagoons, which have relatively steep slopes and low background velocities, and issue previously noted in other studies using sigma coordinates (Shchepetkin and McWilliams, 2009, 2005). While these effects also exist along the forereef slopes, the background currents exhibit much larger values of $O(10$ cm/s) and thus have little effect on the mixing. Since the contribution of the deep lagoons to transport is small, the effect on the model results in the domain outside the deep lagoons is therefore small, and model results are in good agreement with the observations. However, the results for temperature and exchange in the deep lagoons are likely inaccurate. Future models investigating similar low-energy environments should consider this effect if the effects of mixing are important. This overmixing could be improved through increased smoothing of the bathymetry, use of a z-level model (instead of sigma level), and/or a nonhydrostatic model e.g. SUNTANS (Fringer et al., 2006). Outside of these regions, the model temperature profiles are in good agreement with field observations.

Two alternate ways of implementing the 3D wave forcing into the Navier Stokes equations include the traditional radiation stress gradient (Mellor, 2011, 2008), and vortex force formalism (Uchiyama et al., 2010). Several runs were conducted using the radiation stress method; these simulations yielded unrealistically high velocities near the surface by up to a factor of three. This issue was most apparent in locations with shoaling, nonbreaking waves; an issue also noted by Kumar et al. (2011). In contrast, implementation of the vortex force method for this model (Uchiyama et al., 2010) produces realistic vertical velocity profiles and mean flows (Figs. 4 and 6). Thus the vortex force method appears to be the preferred method for modeling the effect of waves on currents in three-dimensions in this environment.

4.2. Interaction of atoll with regional flow

In the presence of a strong easterly regional current on 06-Nov-2012, the atoll creates flow separation and a large wake, which extends a significant distance offshore from the forereef, with shed vortices clearly visible, while in the presence of a northerly regional current on 29-Sep-2013, the wake is less clearly defined but with vortices still present (Fig. 7). In both cases, vortices are shed

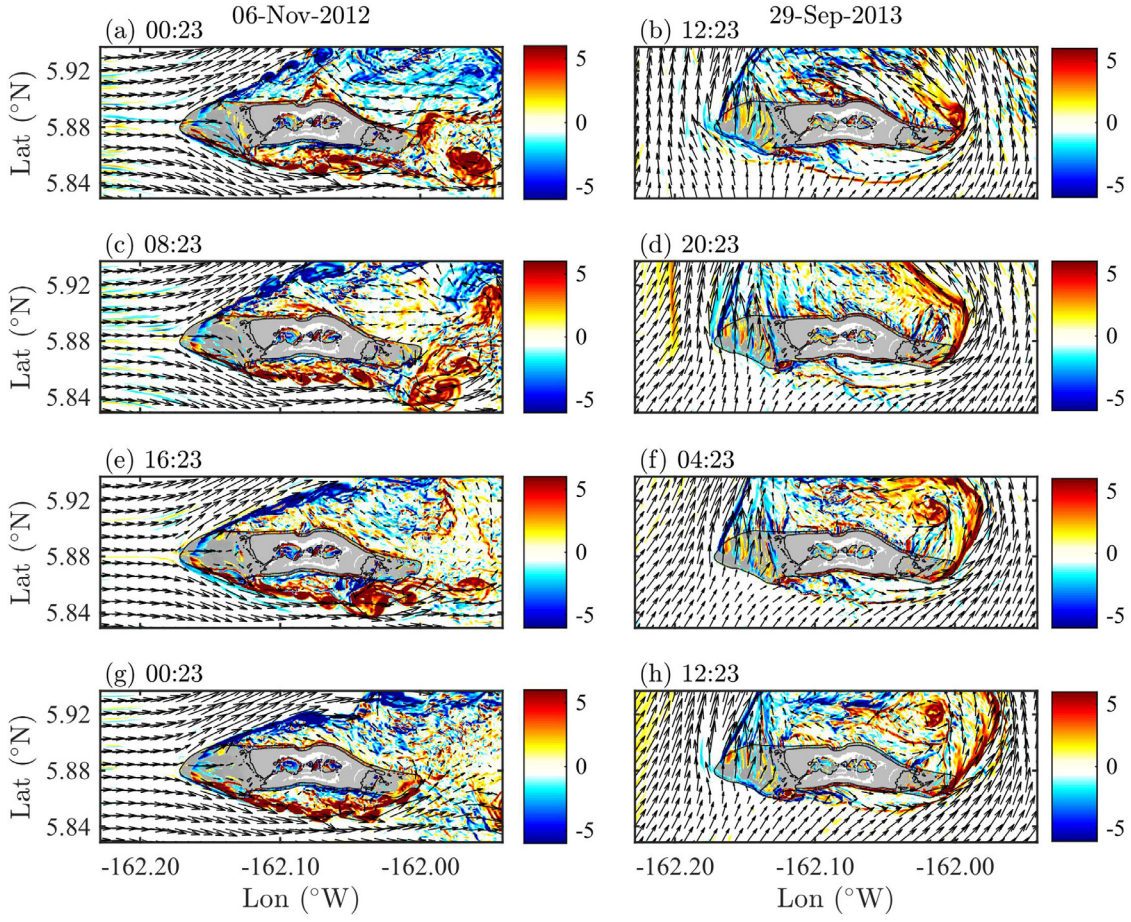

Fig. 7. Regional flow interaction with the atoll, for 24 h sequence starting 06-Nov-2012 (left) and 29-Sep-2013 (right). Black arrows are surface velocity u_s, coloring is surface vorticity ω (10^{-4} 1/s), gray shading is atoll with black lines as 5 and 60 m bathymetric contours. Results only shown for depths greater than 10 m.

from leading edge of the separated region which propagate downstream in the mean flow. At times, these vortices migrate towards the atoll and interact with the forereef, or alternately may spin off into the open ocean. There are also some locations of persistent circulation forced by irregularities in the atoll shape, most notably on the southwest corner of the atoll.

The primary two-dimensional momentum balance at the atoll scale (offshore) is between acceleration (ACC), pressure gradient (PG), and horizontal advection (HA) (Fig. 8),

$$\mathrm{ACC} + \mathrm{HA} = -\mathrm{PG} \tag{5}$$

The model includes only the upper 200 m, and is essentially modeling the upper mixed layer, the depth of which is set by the regional stratification. Thus the flow dynamics are primarily governed by the forcing from the regional flow and its interaction with the geometry of the atoll.

Flow around the atoll appears similar in nature to 2D flow past a cylinder, where the Reynolds number governs the flow. For island wakes, Wolanski et al. (1996) proposed an island wake parameter P, essentially the Reynolds number times the aspect ratio,

$$P = \left(\frac{UL}{K_z}\right)\left(\frac{H}{L}\right)^2, \tag{6}$$

where U is the free stream velocity, L is the island horizontal scale, H is the island vertical scale and K_z is the vertical mixing viscosity. Based on laboratory data, for $P < 1$, there is no wake, for $1 < P < 10$ the wake is stable, and for $P > 10$ vortices are shed from the island (Wolanski et al., 1996). For Palmyra, we assume L varies from 4 to 19 km depending on flow direction, U varies from 0.1 to 0.8 m/s, the upper mixed layer depth H is typically 100 to 200 m, and K_z is typically 0.004 to 0.01 m^2/s in the model. With these assumptions, P would range from 5 to 2000, within the stable wake regime for some conditions, but typically within the unstable vortex shedding regime, consistent with modeling results. For certain conditions such as very low free stream velocity, high mixing, or shallow mixed layer depth, the wake can become stable, an effect which could be studied further. In addition, this simplified model ignores stratification within the upper mixed layer, Coriolis effects, sloping island walls, and bottom stress, all of which could be considered.

4.3. Circulation within atoll

To explain the circulation patterns and dominant forcing mechanisms at smaller scales within the atoll, we look at the depth average momentum budget. Note that within this section, total momentum (i.e. |HA|) is used is used for simplicity instead of the individual vector components, and relative fraction values are the average fraction of total momentum budget (i.e. for term $\overline{X_i} = \overline{|X_i| / \sum_i |X_i|}$).

On the atoll, the significant terms are ACC, HA, PG, HVF, Bstr, Str, and RA depending on the location (Fig. 8). The COR and HM terms are generally not important in driving the 2D flow. The importance of the significant terms is strongly dependent on depth and hydrodynamic regime. The ACC and HS terms are important at most depths greater than 5 m, and the PG term is important at all points in the domain (Fig. 8a,b,d). The Bstr term from the rough reef is important at all depths less than 60 m, while the

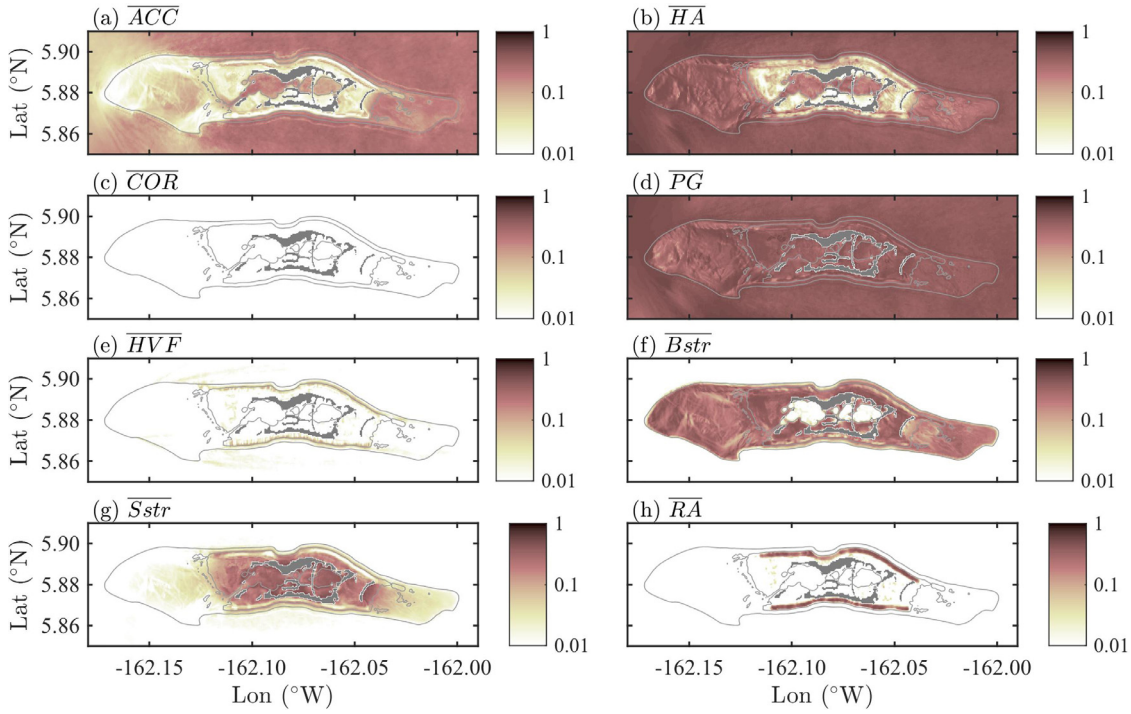

Fig. 8. Relative fraction of contribution from significant 2D momentum terms . (a) acceleration (ACC), (b) horizontal advection (HA), (c) Coriolis (COR), (d) pressure gradient (PG), (e) horizontal vortex force (HVF), (f) bottom stress (Bstr), (g) surface stress (Sstr), and (h) wave roller acceleration (RA). Values are average fraction of total momentum budget during Run 1 (Nov 2012), i.e. for term $\bar{X}_i = \overline{|X_i|/\Sigma_i|X_i|}$, note log scale. Gray lines are 5 and 60 m depth contours; gray shading is land mask.

Str term from wind forcing is important within the interior lagoons and shallow backreefs (Fig. 8f,g). Due to the effect of wave forcing, the RA term is important only within the surf zone, and the HVF is only weakly important in the shoaling region before breaking (Fig. 8e,h). Using these results, the 2D momentum balances in the various hydrodynamic regimes within the atoll can be approximated.

On the forereefs and reef terraces with depths between 5 and 60 m where waves are not often breaking, the balance can be approximated as,

$$\mathrm{ACC} + \mathrm{HA} = -\mathrm{PG} + \mathrm{HVF} - \mathrm{Bstr} + \mathrm{Sstr}, \tag{7}$$

and forcing from tidal flow, regional currents, waves and winds can all be important. However, the Sstr and HVF terms are generally less than 10% of the overall budget.

On the forereef in depths less than 5 m, typically within the surfzone, the balance can be classically approximated as,

$$0 = -\mathrm{PG} - \mathrm{Bstr} + \mathrm{RA}, \tag{8}$$

and consequently, tides creating large scale PG and breaking waves creating RA are the primary driver of flow in this regime. Here, the roller model (RA) accounts for the largest forcing from waves, while the vortex forcing (HVF) is relatively weak.

On the shallow back reefs with depths less than 5 m, the balance can be approximated as,

$$0 = -\mathrm{PG} - \mathrm{Bsrt} + \mathrm{Sstr}, \tag{9}$$

and within the interior lagoons with depth between 5 and 60 m, the balance is approximated as,

$$\mathrm{ACC} + \mathrm{HA} = -\mathrm{PG} + \mathrm{Sstr} \tag{10}$$

Forcing is primarily from winds on the back reef and lagoons, but pressure gradients generated by other processes such as tides and waves can also drive the flow.

Due to the rough and rugose reef, bottom stresses (Bstr) are important at all locations less than 60 m depth on the atoll. Correct parameterization of this effect is critical to accurately modeling flow. For this study, extensive field data at multiple sites allowed for calculation of roughness values (Rogers, 2015), which are consistent with results from other reefs (Lentz et al., 2016; Rosman and Hench, 2011). However, the theory is currently not well developed for selection of roughness values a *priori* from high resolution bathymetric data or other site mapping, and could be considered for future work.

Offshore wave height and direction have a significant effect on the setup and flow within the atoll interior. Waves are sheltered on the lee of atoll and focused on the exterior edges (Fig. 9a,b). Mean free surface setup is highest along the shallow reef flats on the side of the atoll with highest wave height (Fig. 9c,d). Due to these free surface differences, pressure gradients drive flow in the direction of the dominant waves over the reef crest, easterly through the lagoon system, and variably on the eastern and western terraces (Fig. 9e,f). As expected, surface water temperature is lowest during the night (Fig. 9g), and highest during the day (Fig. 9h) on the shallow interior areas, and more stable in the offshore waters.

Tides can modulate the wave-driven flow in shallow areas (Koweek et al., 2015a; Monismith et al., 2013). At high tide, waves drive flow over the reef crest (Fig. 10a), while at low tide, the reef crest is exposed and while the wave forcing is nearly the same, the waves in this case drive an alongshore flow to the northwest and no flow over the crest (Fig. 10b). The net flow over the reef crest q_{crest} generally increases with increasing offshore wave energy flux $\mathcal{F}_{wave}$, but tides modulate this flow such that for a given incoming $\mathcal{F}_{wave}$, q_{crest} is much higher at high tide than low tide (Fig. 10c). A simple model of setup from breaking in the surfzone and friction-pressure gradient on the backreef predicts that $q_{crest} = a\mathcal{F}_{wave}^{1/5} + b$ (Monismith et al., 2013), which is a reasonable fit to the model results with $r^2 = 0.61$ for $a = 0.0855$ and $b = -0.435$.

Average bottom wave stress is highest within the shoaling region and surfzone of the forereef (Fig. 11a). Here, the mean value of the top 2% of near-bed wave velocities squared is employed, a proxy for bottom stress independent of the assumed bottom

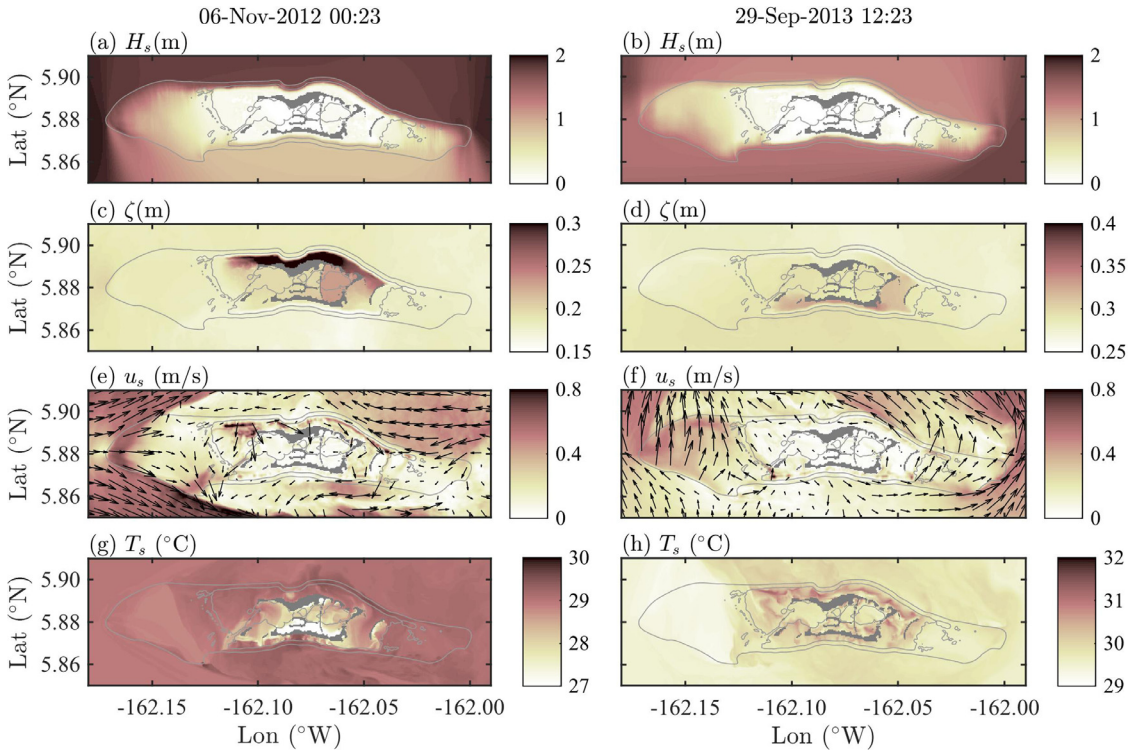

Fig. 9. Atoll scale model results snapshot for time period of nighttime dominant northern waves (left) and daytime dominant southern waves (right). (a,b) significant wave height H_s, (c,d) free surface height $\boldsymbol{\zeta}$, (e,f) surface velocity $\boldsymbol{u_s}$, and (g,h) surface temperature $\boldsymbol{T_s}$. Gray lines are 5 and 60 m depth contours; gray shading is land mask. Note offset in scales for (c-d) and (g-h) is different to account for tidal height and regional temperature respectively.

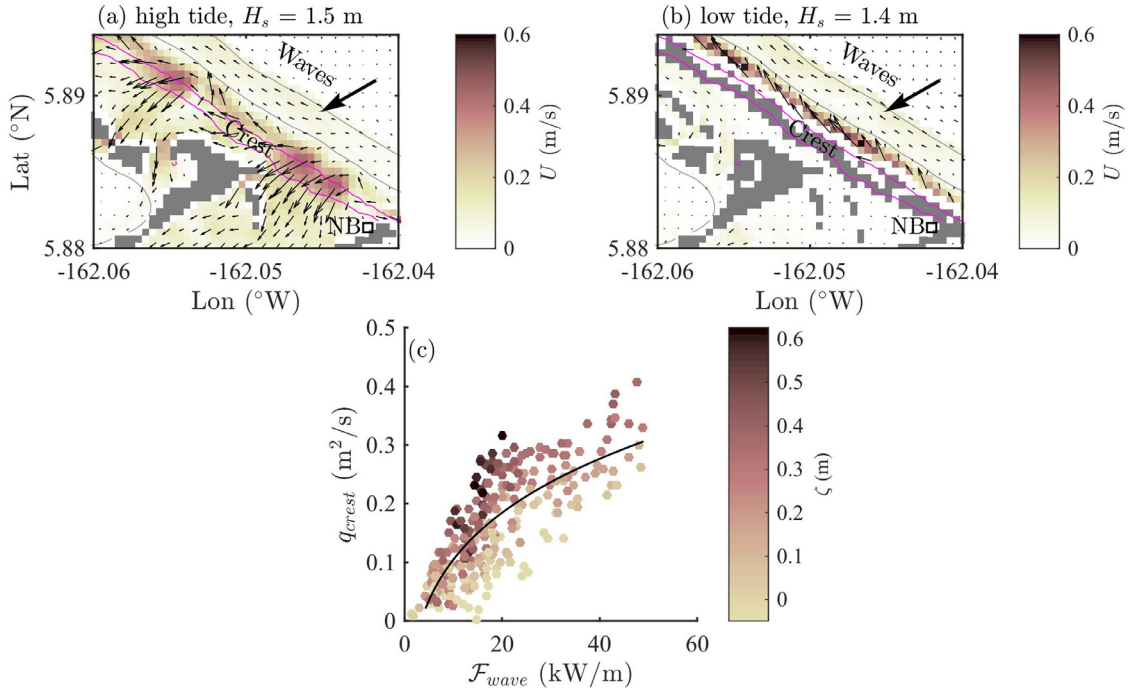

Fig. 10. Tidal modulation of wave-driven flow on northeast corner of atoll during Run 1 (Nov 2012). (a) At high tide, waves drive depth averaged velocity U over the reef crest with significant wave height H_s, while (b) 6 hours previously at low tide and similar H_s, the reef crest is exposed and waves drive flow alongshore on the forereef. (c) Variation of net flow over the reef crest $\boldsymbol{q_{crest}}$, with offshore wave energy flux $\mathcal{F}_{\boldsymbol{wave}}$, and tidal height $\boldsymbol{\zeta}$; line is best fit to the data for $\boldsymbol{q_{crest}} = \boldsymbol{a}\mathcal{F}_{\boldsymbol{wave}}^{1/5} + \boldsymbol{b}$. For (a,b), black arrows show direction of U, gray shading is land mask, gray lines are 5 and 60 m depth contours, and magenta lines are 0.3 m depth contours outlining the reef crest. Location of NB instrument station shown on Fig. 3b for reference.

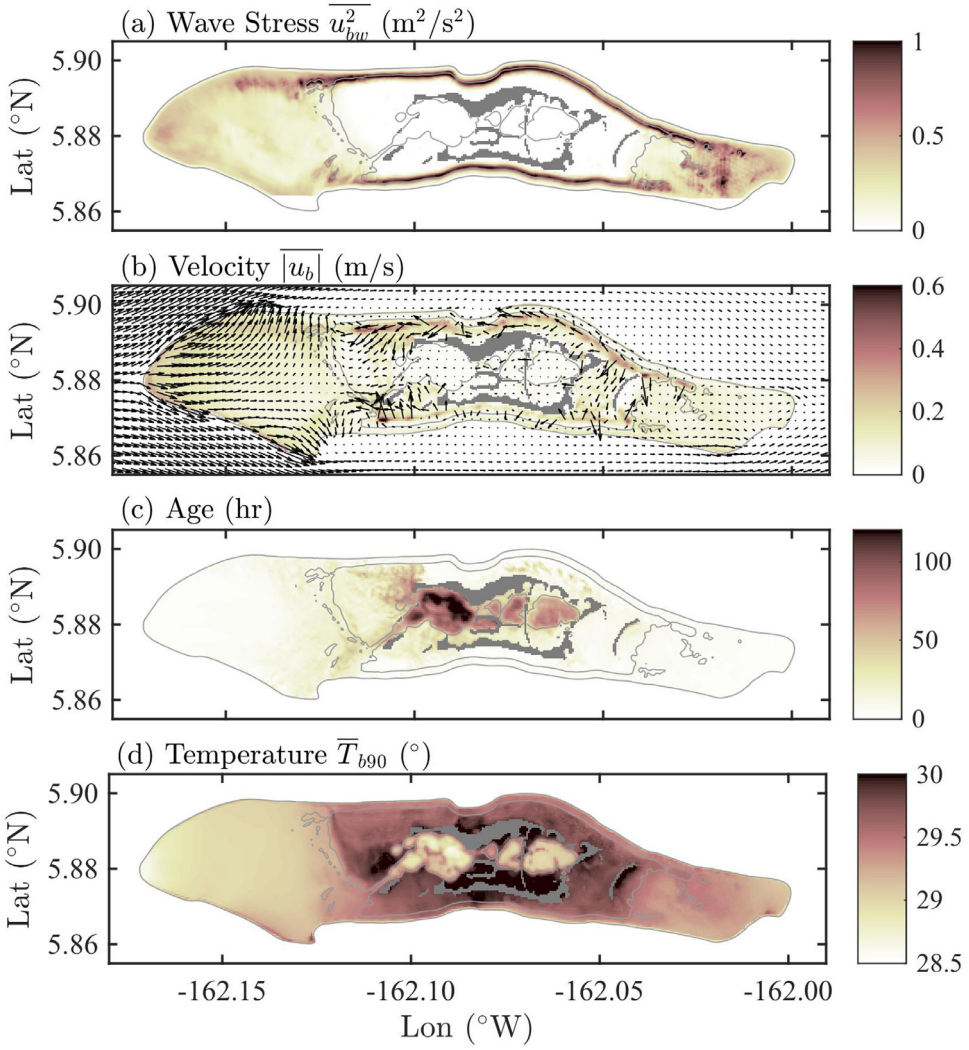

Fig. 11. Model results average bottom wave stress, velocity, age and high temperature. (a) near bottom wave stress proxy $\overline{u_{bw}^2}$, (b) average depth averaged velocity $\bar{\boldsymbol{U}}$ (arrows) and near bottom velocity magnitude $\overline{|\boldsymbol{u_b}|}$ (colors), (c) mean offshore travel time (age), and (d) average of 90th percentile weekly average near bottom temperature $\bar{T}_{b90}$. Averages taken over all model runs. Gray lines are 5 and 60 m depth contours; gray shading is land mask. (For interpretation of the references to colour in this figure legend, the reader is referred to the web version of this article.)

friction (Rogers et al., 2016a). The net long term average circulation shows flow going over the reef crest into the interior of the atoll and in general from east to west within the interior lagoon (Fig. 11b) (average from the four two-week simulations). On the western exterior terraces and forereefs, flow is primarily driven to the east by the regional flow NECC (Fig. 11b). However, individual particle tracks can follow very different flow paths than the mean flows and divergent path from each other due to nonlinear processes such as eddies and dispersion (Fig. 12). For example, particles from the far western terrace (WT W) travel around the atoll to the east predominantly with the mean flow (Fig. 12a). However, particles released on the southwest forereef (FR SW FR3) go predominantly east in the mean flow, but some circle around into the lagoon, while others cross the eastern terrace to the north. Particles released from within the interior lagoon (EL2) follow many divergent paths through the lagoon interior, to the north or south forereefs (Fig. 12h). These results are only a sample from one model run; different mean flow patterns produce different particle tracks.

Using these float tracks over all four runs to calculate travel time from offshore to a point on the atoll (age), the average age is less than 20 hours on the exterior reefs, and up to 120 hours in the interior lagoons (Fig. 11c). Due to the increased mixing in the lagoons from spurious vertical velocities, these results in the lagoons are likely representative of the upper mixed layer. The deep lagoon areas greater than 20 m depth likely have flushing times of 1 to 3 years based on dissolved oxygen profiles (Gardner et al., 2014a). Average high temperatures $\bar{T}_{b90}$ (average of top 90th percentile of weekly average T_b) are lowest on the exterior reefs and deep lagoons and highest on shallow reef flats with low exchange (Fig. 11d).

While the analysis of depth-averaged circulation likely captures the primary mechanisms for flow, density-driven flows may also be important on the atoll. The lagoon system is stratified, and the channel velocity profile and cross-shore flow on the forereefs shows likely evidence of classic baroclinic exchange flow (Rogers et al., 2016b). Shallow water on the reef flats is likely saltier due to differential evaporation and with cooling at night, this water could form bottom density currents which propagate into the interior lagoons or along the exterior forereefs. Thus, further inquiry into density driven flows at the site is warranted.

4.4. Ecological implications and connectivity

One of the primary motivations for undertaking this study is to better understand the role of hydrodynamics in establishing

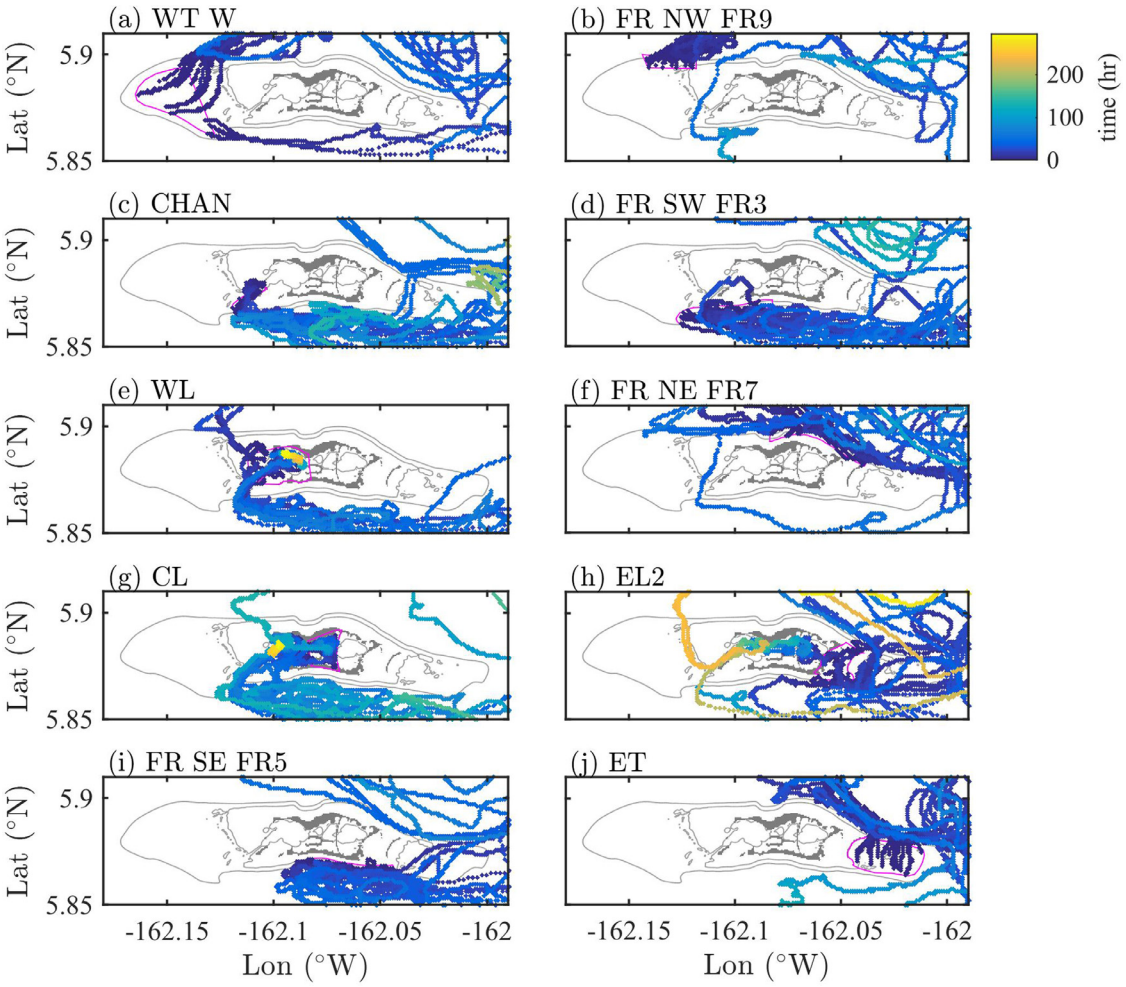

Fig. 12. Selected Lagrangian float tracks for Run 1 (Nov 2012), grouped by starting zone (magenta). Colors are time from float initialization on day 2 (blue), to end of run on day 14 (yellow). Only 20 floats per zone are shown for clarity. Gray lines are 5 and 60 m depth contours; gray shading is land. (For interpretation of the references to colour in this figure legend, the reader is referred to the web version of this article.)

ecological connectivity on the atoll. The Lagrangian connectivity is obtained from the float track model results (Fig. 12) and summarized in Fig. 13a. Overall, the atoll is well connected between regions, and the dominant regions serving as a source are the West Lagoon, Channel and nearby reefs (Fig. 13a,b). Within the atoll interior, primary connectivity is east to west, while on the exterior of the atoll primary connectivity is west to east, consistent with mean flow paths (Fig. 13b). However, limited connectivity occurs between all regions due to tidal phasing, large scale vortices, and other nonlinear effects where individual floats can follow independent tracks which are quite different than the mean flow (Fig. 12). Thus it appears possible for a parcel of water to travel between any region of the atoll for a given set of flow conditions.

It should be noted that this study only considered the connectivity of water parcels passing over each region. Thus, while a parcel of water may pass over a region, it may not be in contact with the bottom, an aspect of the particle trajectory which is of ecological importance for some organisms (e.g.) larval organisms trying to settle on the substrate. Additionally, the Lagrangian floats in these simulations are neutrally carried by the mean velocities, and do not exhibit any swimming patterns, such as exhibited by many larvae (Cowen and Sponaugle, 2009). Additional work could include explicitly modeling different types of larval behavior within the atoll system.

Hydrodynamic properties of interest to coral reef ecosystems include wave stress, light, mean flows, offshore travel time (age), and temperatures, among others. On Palmyra, depth (a proxy for light) has been previously shown to have only a limited effect on coral cover (Rogers et al., 2016a). The limited effect of light is likely because in this clear water low sun angle setting, light zonation is deeper than the extent of benthic mapping (< 20 m depth) (Chappell, 1980).

To evaluate the effect of wave stress, mean flows, age, and temperatures on coral cover, the cumulative probability is used (Fig. 14). Each model grid cell has average hydrodynamic results for average near bottom high wave stress $\overline{u_{bw}^2}$, average near bed velocity $\overline{|u_b|}$, mean travel time (age), and mean of 90th percentile of weekly average temperature $\bar{T}_{b90}$ (Fig. 11); and also a biological cover type (Fig. 1e). The results for each biological cover classification over the entire grid (i.e. Coral $0 < 10\%$) are then presented as the cumulative probability of the hydrodynamic properties. This allows evaluation of how, on average, hydrodynamic properties are distributed in a given biological cover type. If we assume the reef is generally stable, this suggests how hydrodynamic properties may or may not be influencing the reef.

Water motion appears to be beneficial to coral reefs through increasing the rates of nutrient uptake, photosynthetic production and particulate capture (Atkinson and Bilger, 1992; Carpenter et al., 1991; Genin et al., 2009). However, large forces from strong wave

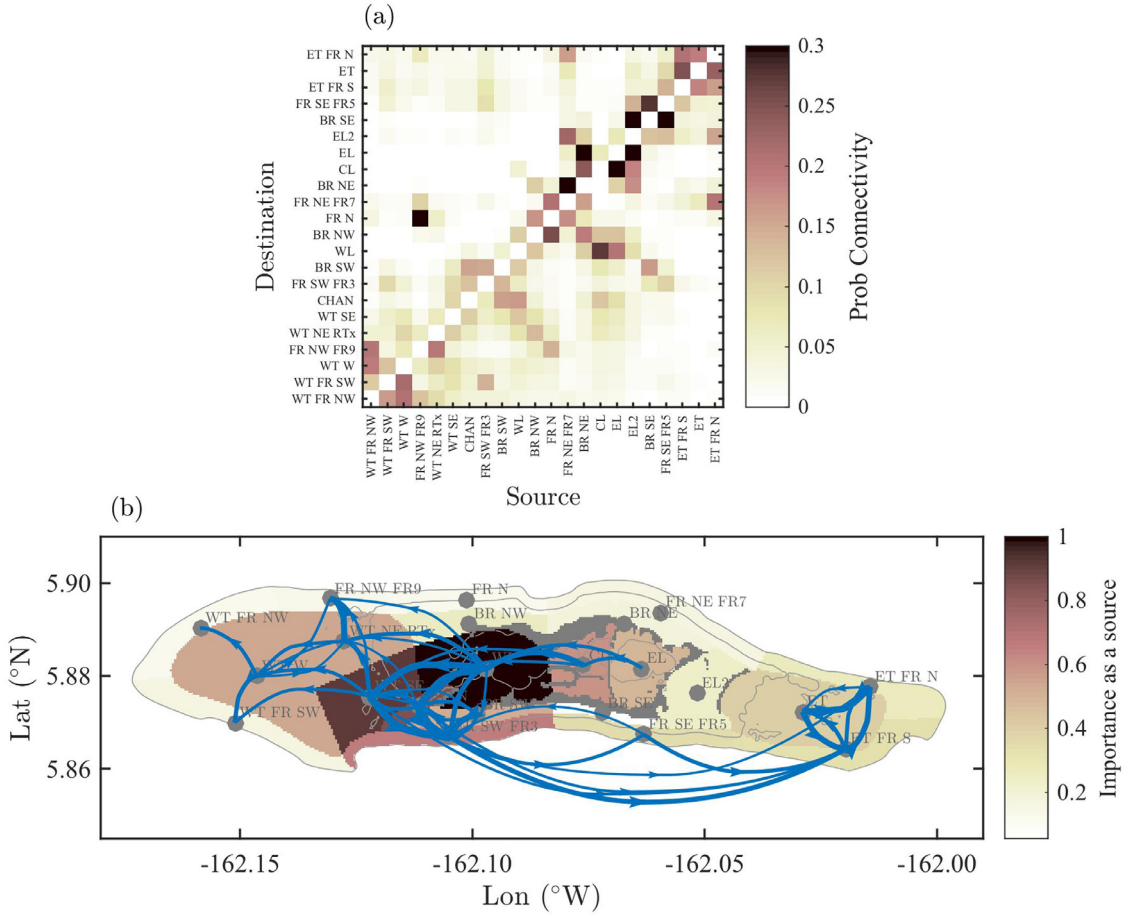

Fig. 13. Connectivity between hydrodynamic zones. (a) connectivity matrix showing the probability a water parcel passing through a destination zone came from a given source zone, and (b) geographic connectivity of top 10% of pathways, where shading is relative importance as an overall source, width of line is relative strength of connection. Results based on average of all model runs; gray shading is land mask, gray lines are 5 and 60 m contours.

motion can subject corals to breakage resulting in trimming or reconfiguration of the reef (Storlazzi et al., 2005). On Palmyra, areas of high coral cover (>50%) are generally associated with moderate wave stress, suggestive of this balance between nutrient supply and reduction in breakage, and the importance of wave stress on the benthic community (Fig. 14a) (Rogers et al., 2016a).

The near bed mean flows are nearly similar for all biological cover types, with some preference for higher flows for the highest coral cover areas (>50%) (Fig. 14b). Therefore, mean flows appear to only be weakly associated with higher coral cover at this site.

Offshore travel time (age) is defined as the average time taken for offshore water to come to a particular point on the atoll. This metric likely includes the effect of multiple processes on the reef, notably water quality and temperature. The longer a parcel of water spends in the atoll system, the greater the effects from changes in nutrients, oxygen, alkalinity, pH, compared to offshore waters. At this site, areas with moderate to high coral cover (> 10%) are generally associated with low water age, while areas with low coral cover (> 10%) are associated with high water age (Fig. 14c). The deep lagoon waters are known to be regularly anoxic and sulphidic, conditions which are detrimental to corals (Gardner et al., 2014a). The longer a parcel spends in the atoll system, the more it is subjected to the local heating effects, as compared to the relatively stable offshore water temperatures. The effect of age on biological cover is likely mostly a function of temperature and to a lesser extent water quality (i.e., nutrients, oxygen, alkalinity, and/or pH).

Temperature variations are well-known to influence coral reefs which have experienced global declines resulting from bleaching events caused by week to month long warm water exposure (Carpenter et al., 2008; Hughes et al., 2003). However, corals can often resist high temperature variability at hourly timescales (Dandan et al., 2015; Mayfield et al., 2013), and the spatial variations in coral cover appear to be most correlated to temperature variations on time scales of days to weeks (Rogers et al., 2016b). These model results show areas with high coral cover (> 50%) associated with lower weekly temperatures, while sites with low coral cover (< 10%) are associated with high weekly temperatures (Fig. 14d). These results agree with previous findings from multi-year field observations on Palmyra (Rogers et al., 2016b).

In general, areas of high coral cover (> 50%) are associated with moderate wave stress, lower age, and lower temperature, while areas of very low coral cover (< 10%) are associated with high water age and high temperature. Thus, moderate wave stress, low water age, and lower temperatures appear to be part of the suite of conditions necessary for high coral cover at this site. Corals at this site are close to their high thermal limit (Rogers et al., 2016b; Williams et al., 2010), and so temperature has a strong effect on coral zonation. Interestingly, Rogers et al. (2016b) found that the physical factors favoring high coral cover percentage varied according to the different prevailing hydrodynamic regimes: low temperatures in backreef habitats, short travel times in lagoon habitats (days since entering the reef system), and lower wave stress on forereef habitats, a pattern which is likely present here too.

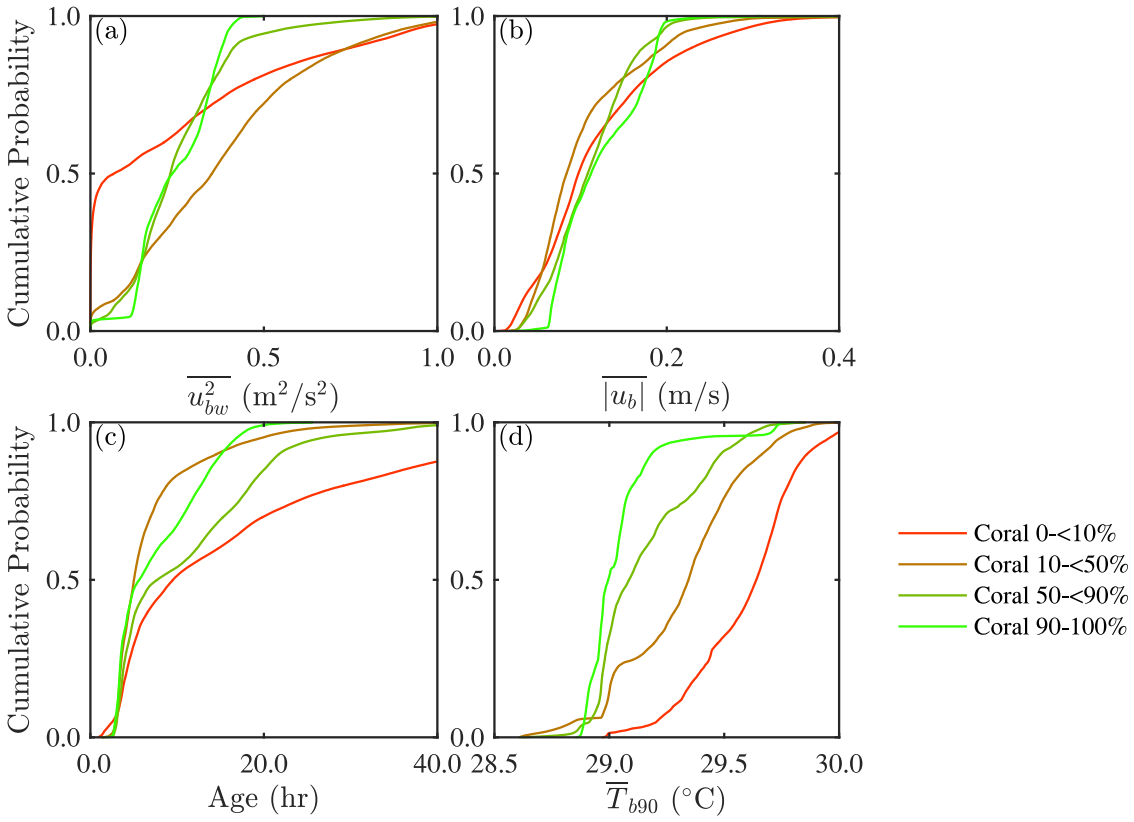

Fig. 14. Cumulative probability of biological cover as a function of average near bottom wave stress, near bottom velocity, water age, and high weekly temperature. Biological cover with (a) near bottom wave stress proxy $\overline{u_{bw}^2}$, (b) average near bottom velocity $\overline{|u_b|}$, (c) offshore travel time (age), and (d) 90th percentile of weekly average near bottom temperature $\bar{T}_{b90}$. Results are average over all model runs.

Rogers et al. (2016b) also note that light of future warming from climate change, local areas of reefs which maintain lower temperatures through wave-driven mean flows will have the best likelihood of promoting coral survival, a conclusion also supported by these results.

5. Conclusions

We present results from modeling simulations using a coupled wave and three-dimensional hydrodynamic model (COAWST) applied to Palmyra Atoll. This study is the first time that the vortex force formalism has been implemented in an environment with very high bottom drag. In addition, the model uses a modified bottom friction formulation in the SWAN wave model (Rogers et al., 2016a) to account for the high bottom friction characteristic of this setting and likely many other tropical atolls. Considering the model complexity in terms of bathymetry, bottom roughness, and forcing (waves, wind, metrological, tides, regional boundary conditions), and open boundary conditions from a global model, the results for depth averaged quantities, tides, and vertical structure are in good agreement with the field observations. The model over predicts mixing in the deep lagoons due to spurious vertical velocities, and over predicts exchange in the East Lagoon due to poorly resolved inlets. Outside of these regions, the model results are in good agreement with field observations. Future model development in similar environments should carefully consider the bathymetry in areas of hydrodynamic controls and correct bottom stress parameterization.

At the atoll scale, strong regional flows create flow separation and a well-defined wake, similar to 2D flow past a cylinder, and consistent with previous work on island wakes. Vortices are shed from the leading edge of the wake, which can interact with the atoll and enhance connectivity by redistributing waters across different regions.

Momentum balances indicate the important forcing mechanisms, and are strongly a function of depth and hydrodynamic regime. Bottom stress is a significant term in the momentum balance everywhere for depths less than 60 m. Circulation within the atoll is generally driven by waves over the reef crest and from east to west within the interior lagoon system, and this wave-driven flow is modulated by the tides in areas of shallow depth.

The Lagrangian connectivity is obtained from the float track model results. The resulting connectivity within the atoll system shows that the general trends follow the mean flow paths, i.e. from west to east on the atoll exterior reefs and from east to west within the interior lagoon system. However, some connectivity exists between all regions of the atoll system, due to tidal phasing, vortices and other nonlinear interactions.

Moderate wave stress, short travel time (days since entering the reef system), and low temperature appear to be the most ideal conditions for high coral cover at this site. Corals at this site are close to their high thermal limit (Rogers et al., 2016b; Williams et al., 2010), and so temperature has a strong effect on coral zonation. The effect of travel time on biological cover is likely mostly a function of temperature and to a lesser extent water quality. In light of future warming from climate change, local areas of reefs which maintain lower temperatures through wave-driven mean flows will have the best likelihood of promoting coral survival

Future work could examine the effects of density driven flow, which are likely important in some regions of the atoll such as the interior lagoons and outlet channels. Additional work could explicitly model larval connectivity, considering vertical location in the water column and larval swimming patterns. Finally, for this study, extensive field data at multiple sites allowed for calculation

of roughness values to parameterize the model. Development of methods for selection of roughness values a *priori* from high resolution bathymetric data or other site mapping would warrant further inquiry.

Acknowledgements

We thank Matthew Rayson, Sean Vitousek, and John Warner for assistance with modeling. Bathymetry and other information were provided by Jamison Gove. Research funding was provided by Stanford University along with two grants from the Gordon and Betty Moore Foundation ("Observations and modeling of the C system dynamics at Palmyra Atoll: In support of the development of management strategies for ocean acidification impacts in the tropics," to RBD and, "Understanding coral reef resilience to advance science and conservation," to RBD and SGM), as well as a grant from the National Science Foundation OCE-1536502 ("Collaborative Research: Wave driven flow through a shallow, fringing reef" to SGM). This research was accomplished with government support under and awarded by the U.S. Department of Defense, Office of Naval Research, NDSEG Fellowship, 32 CFR 168a to JSR. DAK was funded by an NSF Graduate Research Fellowship. This is Palmyra Atoll Research Consortium contribution number PARC-0127.

References

Acevedo, R., Morelock, J., Olivieri, R., 1989. Modification of coral reef zonation by terrigenous sediment stress. Palaios 4, 92–100.

Andréfouët, S., Ardhuin, F., Queffeulou, P., Le Gendre, R., 2012. Island shadow effects and the wave climate of the Western Tuamotu Archipelago (French Polynesia) inferred from altimetry and numerical model data. Mar. Pollut. Bull. 65, 415–424. doi:10.1016/j.marpolbul.2012.05.042.

Andréfouët, S., Mumby, P., McField, M., Hu, C., Muller-Karger, F., 2002. Revisiting coral reef connectivity. Coral Reefs 21, 43–48. doi:10.1007/s00338-001-0199-0.

Andréfouët, S., Ouillon, S., Brinkman, R., Falter, J., Douillet, P., Wolk, F., Smith, R., Garen, P., Martinez, E., Laurent, V., Lo, C., Remoissenet, G., Scourzic, B., Gilbert, a, Deleersnijder, E., Steinberg, C., Choukroun, S., Buestel, D., 2006. Review of solutions for 3D hydrodynamic modeling applied to aquaculture in South Pacific atoll lagoons. Mar. Pollut. Bull. 52, 1138–1155. doi:10.1016/j.marpolbul.2006.07.014.

Arístegui, J., Sangrá, P., Hernández-León, S., Cantón, M., Hernández-Guerra, A., Kerling, J.L., 1994. Island-induced eddies in the Canary islands. Deep Sea Res. Part I 41, 1509–1525. doi:10.1016/0967-0637(94)90058-2.

Atkinson, M.J., Bilger, R.W., 1992. Effects of water velocity on phosphate uptake in coral reef-flat communities. Limnol. Ocean 37, 273–279. doi:10.4319/lo.1992.37.2.0273.

Atkinson, M.J., Smith, S.V., Stroup, E.D., 1981. Circulation in Enewetak Atoll lagoon. Limnol. Oceanogr. 26, 1074–1083. doi:10.4319/lo.1981.26.6.1074.

Booij, N., Ris, R.C., Holthuijsen, L.H., 1999. A third-generation wave model for coastal regions: 1. Model description and validation. J. Geophys. Res. 104, 7649–7666. doi:10.1029/98JC02622.

Buddemeier, R.W., Hopley, D., 1988. Turn-ons and turn-offs: causes and mechanisms of the initiation and termination of coral reef growth. International Coral Reef Symposium.

Burke, L., Reytar, K., Spalding, M., Perry, A., 2011. Reefs at Risk Revisited. World Resources Institute, Washington DC.

Callaghan, D.P., Nielsen, P., Cartwright, N., Gourlay, M.R., Baldock, T.E., 2006. Atoll lagoon flushing forced by waves. Coast. Eng. 53, 691–704. doi:10.1016/j.coastaleng.2006.02.006.

Carpenter, K.E., Abrar, M., Aeby, G., Aronson, R.B., Banks, S., Bruckner, A., Chiriboga, A., Cortés, J., Delbeek, J.C., Devantier, L., Edgar, G.J., Edwards, A.J., Fenner, D., Guzmán, H.M., Hoeksema, B.W., Hodgson, G., Johan, O., Licuanan, W.Y., Livingstone, S.R., Lovell, E.R., Moore, J.A., Obura, D.O., Ochavillo, D., Polidoro, B.A., Precht, W.F., Quibilan, M.C., Reboton, C., Richards, Z.T., Rogers, A.D., Sanciangco, J., Sheppard, A., Sheppard, C., Smith, J., Stuart, S., Turak, E., Veron, J.E.N., Wallace, C., Weil, E., Wood, E., 2008. One-third of reef-building corals face elevated extinction risk from climate change and local impacts. Science 321, 560–563. doi:10.1126/science.1159196.

Carpenter, R.C., Hackney, J.M., Adey, W.H., 1991. Measurements of primary productivity and nitrogenase activity of coral reef algae in a chamber incorporating oscillatory flow. Limnol. Oceanogr. 36, 40–49. doi:10.4319/lo.1991.36.1.0040.

Chappell, J., 1980. Coral morphology, diversity and reef growth. Nature 286, 249–252. doi:10.1038/286249a0.

Cowen, R.K., Sponaugle, S., 2009. Larval dispersal and marine population connectivity. Ann. Rev. Mar. Sci. 1, 443–466. doi:10.1146/annurev.marine.010908.163757.

Craik, A.D.D., Leibovich, S., 1976. A rational model for Langmuir circulations. J. Fluid Mech. 73, 401. doi:10.1017/S0022112076001420.

Dandan, S.S., Falter, J.L., Lowe, R.J., McCulloch, M.T., 2015. Resilience of coral calcification to extreme temperature variations in the Kimberley region, northwest Australia. Coral Reefs 34, 1151–1163. doi:10.1007/s00338-015-1335-6.

Darwin, C.H., 1842. The Structure and Distribution of Coral Reefs.. Smith, Elder and Co., London.

Delesalle, B., Sournia, A., 1992. Residence time of water and phytoplankton biomass in coral reef lagoons. Cont. Shelf Res. 12, 939–949. doi:10.1016/0278-4343(92)90053-M.

Douillet, P., Ouillon, S., Cordier, E., 2001. A numerical model for fine suspended sediment transport in the southwest lagoon of New Caledonia. Coral Reefs 20, 361–372. doi:10.1007/s00338-001-0193-6.

Dumas, F., Le Gendre, R., Thomas, Y., Andréfouët, S., 2012. Tidal flushing and wind driven circulation of Ahe atoll lagoon (Tuamotu Archipelago, French Polynesia) from in situ observations and numerical modelling. Mar. Pollut. Bull. 65, 425–440. doi:10.1016/j.marpolbul.2012.05.041.

Egbert, G.D., Erofeeva, S.Y., 2002. Efficient inverse modeling of Barotropic ocean tides. J. Atmos. Ocean. Technol. 19, 183–204. doi:10.1175/1520-0426(2002)019⟨0183:EIMOBO⟩2.0.CO;2.

Fabricius, K.E., 2005. Effects of terrestrial runoff on the ecology of corals and coral reefs: review and synthesis. Mar. Pollut. Bull. 50, 125–146. doi:10.1016/j.marpolbul.2004.11.028.

Fringer, O.B., Gerritsen, M., Street, R.L., 2006. An unstructured-grid, finite-volume, nonhydrostatic, parallel coastal ocean simulator. Ocean Model. 14, 139–173. doi:10.1016/j.ocemod.2006.03.006.

Gardner, J.P.A., Garton, D.W., Collen, J.D., Zwartz, D., 2014a. Distant storms as drivers of environmental change at Pacific atolls. PLoS One 9, e87971. doi:10.1371/journal.pone.0087971.

Gardner, J.P.A., John Bartz, R., Brainard, R.E., Collen, J.D., Dunbar, R.B., Garton, D.W., Powell, S., 2014b. Conservation management options and actions: putative decline of coral cover at Palmyra Atoll, Northern Line Islands, as a case study. Mar. Pollut. Bull. 84, 182–190. doi:10.1016/j.marpolbul.2014.05.013.

Genin, A., Monismith, S.G., Reidenbach, M.A., Yahel, G., Koseff, J.R., 2009. Intense benthic grazing of phytoplankton in a coral reef. Limnol. Oceanogr. 54, 938–951. doi:10.4319/lo.2009.54.3.0938.

Haidvogel, D.B., Arango, H., Budgell, W.P., Cornuelle, B.D., Curchitser, E., Di Lorenzo, E., Fennel, K., Geyer, W.R., Hermann, A.J., Lanerolle, L., Levin, J., McWilliams, J.C., Miller, A.J., Moore, A.M., Powell, T.M., Shchepetkin, A.F., Sherwood, C.R., Signell, R.P., Warner, J.C., Wilkin, J., 2008. Ocean forecasting in terrain-following coordinates: formulation and skill assessment of the regional ocean modeling system. J. Comput. Phys. 227, 3595–3624. doi:10.1016/j.jcp.2007.06.016.

Hench, J., Leichter, J.J., Monismith, S.G., 2008. Episodic circulation and exchange in a wave-driven coral reef and lagoon system. Limnol. Oceanogr. 53, 2681–2694.

Hoegh-Guldberg, O., Mumby, P.J.P.J., Hooten, A.J.J., Stenack, R.S., Greenfield, P., Gomez, E., Harvell, C.D.D., Sale, P.F., Edwards, A.J., Caldeira, K., Knowlton, N., Eakin, C.M., Inglesias-Priesto, R., Muthiga, N., Bradbury, R.H., Dubi, A., Hatziolos, M.E.E., Steneck, R.S., Greenfield, P., Gomez, E., Harvell, C.D.D., Sale, P.F., Edwards, A.J., Caldeira, K., Knowlton, N., Eakin, C.M., Iglesias-Prieto, R., Muthiga, N., Bradbury, R.H., Dubi, A., Hatziolos, M.E.E., 2007. Coral reefs under rapid climate change and ocean acidification. Science 318, 1737–1742. doi:10.1126/science.1152509.

Hoeke, R.K., Storlazzi, C.D., Ridd, P.V., 2013. Drivers of circulation in a fringing coral reef embayment: a wave-flow coupled numerical modeling study of Hanalei Bay, Hawaii. Cont. Shelf Res. 58, 79–95. doi:10.1016/j.csr.2013.03.007.

Hsin, Y.-C.C., Qiu, B., 2012. Seasonal fluctuations of the surface North Equatorial Countercurrent (NECC) across the Pacific basin. J. Geophys. Res. Ocean. 117, 1–17. doi:10.1029/2011JC007794.

Hughes, T.P., Baird, A.H., Bellwood, D.R., Card, M., Connolly, S.R., Folke, C., Grosberg, R., Hoegh-Guldberg, O., Jackson, J.B.C., Kleypas, J., Lough, J.M., Marshall, P., Nyström, M., Palumbi, S.R., Pandolfi, J.M., Rosen, B., Roughgarden, J., 2003. Climate change, human impacts, and the resilience of coral reefs. Science 301, 929–933. doi:10.1126/science.1085046.

Jones, G.P., Almany, G.R., Russ, G.R., Sale, P.F., Steneck, R.S., van Oppen, M.J.H., Willis, B.L., 2009. Larval retention and connectivity among populations of corals and reef fishes: history, advances and challenges. Coral Reefs 28, 307–325. doi:10.1007/s00338-009-0469-9.

Kench, P.S., 1998. Physical processes in a semi-enclosed Indian Ocean. Coral Reefs 17, 13.

Kleypas, J.A., 1999. Geochemical consequences of increased atmospheric carbon dioxide on coral reefs. Science 284, 118–120. doi:10.1126/science.284.5411.118.

Koweek, D.A., Dunbar, R.B., Monismith, S.G., Mucciarone, D.A., Woodson, C.B., Samuel, L., 2015a. High-resolution physical and biogeochemical variability from a shallow back reef on Ofu, American Samoa: an end-member perspective. Coral Reefs. doi:10.1007/s00338-015-1308-9.

Koweek, D.A., Dunbar, R.B., Rogers, J.S., Williams, G.J., Price, N., Mucciarone, D.A., Teneva, L., 2015b. Environmental and ecological controls of coral community metabolism on Palmyra Atoll. Coral Reefs 34, 339–351. doi:10.1007/s00338-014-1217-3.

Kraines, S., Yanagi, T., Isobe, M., Komiyama, H., 1998. Wind-wave driven circulation on the coral reef at Bora Bay, Miyako Island. Coral Reefs 17, 133–143. doi:10.1007/s003380050107.

Kumar, N., Feddersen, F., Uchiyama, Y., McWilliams, J.C., O'Reilly, W., 2015. Midshelf to surfzone coupled ROMS–SWAN model data comparison of waves, currents, and temperature: diagnosis of subtidal forcings and response. J. Phys. Oceanogr. 45, 1464–1490. doi:10.1175/JPO-D-14-0151.1.

Kumar, N., Voulgaris, G., Warner, J.C., Olabarrieta, M., 2012. Implementation of the vortex force formalism in the coupled ocean-atmosphere-wave-sediment transport (COAWST) modeling system for inner shelf and surf zone applications. Ocean Model. 47, 65–95. doi:10.1016/j.ocemod.2012.01.003.

Kumar, N., Voulgaris, G., Warner, J.C.C., 2011. Implementation and modification of a three-dimensional radiation stress formulation for surf zone and rip-current applications. Coast. Eng. 58, 1097–1117. doi:10.1016/j.coastaleng.2011.06.009.

Lentz, S.J., Churchill, J.H., Davis, K.A., Farrar, J.T., Pineda, J., Starczak, V., 2016. The characteristics and dynamics of wave-driven flow across a platform coral reef in the Red Sea. J. Geophys. Res. Ocean. doi:10.1002/2015JC011141.

Longuet-Higgins, M.S., Stewart, R.w., 1964. Radiation stresses in water waves; a physical discussion, with applications. Deep Sea Res. Oceanogr. Abstr. 11, 529–562. doi:10.1016/0011-7471(64)90001-4.

Lowe, R.J., Falter, J.L., 2015. Oceanic forcing of coral reefs. Ann. Rev. Mar. Sci. 7, 43–66. doi:10.1146/annurev-marine-010814-015834.

Lowe, R.J., Falter, J.L., Monismith, S.G., Atkinson, M.J., 2009a. A numerical study of circulation in a coastal reef-lagoon system. J. Geophys. Res. Ocean. 114, 1–18. doi:10.1029/2008JC005081.

Lowe, R.J., Falter, J.L., Monismith, S.G., Atkinson, M.J., 2009b. Wave-driven circulation of a coastal reef – lagoon system. J. Phys. Oceanogr. 39, 873–893. doi:10.1175/2008JPO3958.1.

Lugo-Fernández, A., Roberts, H.H., Wiseman, W.J., 2004. Currents, water levels, and mass transport over a modern Caribbean coral reef: tague reef, St. Croix. USVI. Cont. Shelf Res. 24, 1989–2009. doi:10.1016/j.csr.2004.07.004.

Maragos, J.E., Friedlander, A.M., Godwin, S., Musburger, C., Tsuda, R., Flint, E., Pantos, O., Ayotte, P., Sala, E., Sandin, S., McTee, S., Siciliano, D., Obura, D., 2008. US coral reefs in the Line and Phoenix Islands, central Pacific Ocean: status, threats and significance. In: Coral Reefs USA, pp. 643–654.

Mayfield, A.B., Chen, M.N., Meng, P.J., Lin, H.J., Chen, C.S., Liu, P.J., 2013. The physiological response of the reef coral Pocillopora damicornis to elevated temperature: Results from coral reef mesocosm experiments in Southern Taiwan. Mar. Environ. Res. 86, 1–11. doi:10.1016/j.marenvres.2013.01.004.

Mellor, G., 2011. Wave radiation stress. Ocean Dyn. 61, 563–568. doi:10.1007/s10236-010-0359-2.

Mellor, G.L., 2008. The depth-dependent current and wave interaction equations: a revision. J. Phys. Oceanogr. 38, 2587–2596. doi:10.1175/2008JPO3971.1.

Monismith, S.G., 2007. Hydrodynamics of coral reefs. Annu. Rev. Fluid Mech. 39, 37–55. doi:10.1146/annurev.fluid.38.050304.092125.

Monismith, S.G., Genin, A., Reidenbach, M.a., Yahel, G., Koseff, J.R., 2006. Thermally driven exchanges between a coral reef and the adjoining ocean. J. Phys. Oceanogr. 36, 1332–1347. doi:10.1175/JPO2916.1.

Monismith, S.G., Herdman, L.M.M., Ahmerkamp, S., Hench, J.L., 2013. Wave transformation and wave-driven flow across a steep coral reef. J. Phys. Oceanogr. 43, 1356–1379. doi:10.1175/JPO-D-12-0164.1.

Monismith, S.G., Rogers, J.S., Koweek, D.A., Dunbar, R.B., 2015. Frictional wave dissipation on a remarkably rough reef. Geophys. Res. Lett. 42, 1–9. doi:10.1002/2015GL063804.

Monsen, N.E., Cloern, J.E., Lucas, L.V., Monismith, S.G., 2002. The use of flushing time, residence time, and age as transport time scales. Limnol. Oceanogr. 47, 1545–1553. doi:10.4319/lo.2002.47.5.1545.

Munk, W.H., Sargent, M.C., 1954. Adjustment of Bikini Atoll to ocean waves. U. S. Geol. Sur. Prof. Paper 260-C.

Odum, H.T., Odum, E.P., 1955. Trophic structure and productivity of a windward coral reef community on eniwetok atoll. Ecol. Monogr. 25, 291–320.

Palumbi, S.R., Barshis, D.J., Traylor-Knowles, N., Bay, R.A., 2014. Mechanisms of reef coral resistance to future climate change. Science 344, 895–898.

Riegl, B., Dodge, R., 2008. Coral Reefs of the USA. Elsevier doi:10.1007/978-1-4020-6847-8.

Roberts, C.M., 1997. Connectivity and management of Caribbean coral reefs. Science 278, 1454–1457. doi:10.1126/science.278.5342.1454.

Rogers, C.S.C., 1990. Responses of coral reefs and reef organisms to sedimentation. Mar. Ecol. Prog. Ser. 62, 185–202. doi:10.3354/meps062185.

Rogers, J.S., 2015. Physical Oceanography in Coral Reef Environments Wave and Mean Flow Dynamics at Small and Large Scales, and Resulting Ecological Implications. Stanford University.

Rogers, J.S., Monismith, S.G., Dunbar, R.B., Koweek, D.A., 2015. Field observations of wave-driven circulation over spur and groove formations on a coral reef. J. Geophys. Res. 120, 145–160. doi:10.1002/2014JC010464.

Rogers, J.S., Monismith, S.G., Koweek, D.A., Dunbar, R.B., 2016a. Wave dynamics of a Pacific Atoll with high frictional effects. J. Geophys. Res. 121, 350–367. doi:10.1002/2015JC011170.

Rogers, J.S., Monismith, S.G., Koweek, D.A., Torres, W.I., Dunbar, R.B., 2016b. Thermodynamics and hydrodynamics in an atoll reef system and their influence on coral cover. Limnol. Oceanogr. doi:10.1002/lno.10365.

Rosman, J.H., Hench, J.L., 2011. A framework for understanding drag parameterizations for coral reefs. J. Geophys. Res. Ocean. 116, 1–15. doi:10.1029/2010JC006892.

Sandin, S.A., Smith, J.E., Demartini, E.E., Dinsdale, E.A., Donner, S.D., Friedlander, A.M., Konotchick, T., Malay, M., Maragos, J.E., Obura, D., Pantos, O., Paulay, G., Richie, M., Rohwer, F., Schroeder, R.E., Walsh, S., Jackson, J.B.C., Knowlton, N., Sala, E., 2008. Baselines and degradation of coral reefs in the northern line islands. PLoS One 3, e1548. doi:10.1371/journal.pone.0001548.

Shchepetkin, A.F., McWilliams, J.C., 2009. Correction and commentary for "Ocean forecasting in terrain-following coordinates: Formulation and skill assessment of the regional ocean modeling system" by Haidvogel et al., J. Comp. Phys. 227, pp. 3595–3624. J. Comput. Phys. 228, 8985–9000. doi:10.1016/j.jcp.2009.09.002.

Shchepetkin, A.F., McWilliams, J.C., 2005. The regional oceanic modeling system (ROMS): a split-explicit, free-surface, topography-following-coordinate oceanic model. Ocean Model 9, 347–404. doi:10.1016/j.ocemod.2004.08.002.

Shchepetkin, A.F., McWilliams, J.C., 2003. A method for computing horizontal pressure-gradient force in an oceanic model with a nonaligned vertical coordinate. J. Geophys. Res. 108. doi:10.1029/2001JC001047, 3090–.

Stevenson, C., Katz, L.S., Micheli, F., Block, B., Heiman, K.W., Perle, C., Weng, K., Dunbar, R.B., Witting, J., 2007. High apex predator biomass on remote Pacific islands. Coral Reefs 26, 47–51. doi:10.1007/s00338-006-0158-x.

Stevenson, S., Powell, B.S., Merrifield, M.A., Cobb, K.M., Nusbaumer, J., Noone, D., 2015. Characterizing seawater oxygen isotopic variability in a regional ocean modeling framework: implications for coral proxy records. Paleoceanography 30, 1573–1593. doi:10.1002/2015PA002824.

Storlazzi, C.D., Brown, E.K., Field, M.E., Rodgers, K., Jokiel, P.L., 2005. A model for wave control on coral breakage and species distribution in the Hawaiian Islands. Coral Reefs 24, 43–55. doi:10.1007/s00338-004-0430-x.

Symonds, G., Black, K.P., Young, I.R., 1995. Wave-driven flow over shallow reefs. J. Geophys. Res. 100, 2639. doi:10.1029/94JC02736.

Uchiyama, Y., McWilliams, J.C., Shchepetkin, A.F., 2010. Wave-current interaction in an oceanic circulation model with a vortex-force formalism: Application to the surf zone. Ocean Model 34, 16–35. doi:10.1016/j.ocemod.2010.04.002.

Warner, J.C., Armstrong, B., He, R., Zambon, J.B., 2010. Development of a Coupled Ocean–Atmosphere–Wave–Sediment Transport (COAWST) modeling system. Ocean Model. 35, 230–244. doi:10.1016/j.ocemod.2010.07.010.

Warner, J.C., Sherwood, C.R., Arango, H.G., Signell, R.P., 2005. Performance of four turbulence closure models implemented using a generic length scale method. Ocean Model. 8, 81–113. doi:10.1016/j.ocemod.2003.12.003.

Williams, G.J., Knapp, I.S., Maragos, J.E., Davy, S.K., 2010. Modeling patterns of coral bleaching at a remote Central Pacific atoll. Mar. Pollut. Bull. 60, 1467–1476. doi:10.1016/j.marpolbul.2010.05.009.

Williams, G.J., Smith, J.E., Conklin, E.J., Gove, J.M., Sala, E., Sandin, S.A., 2013. Benthic communities at two remote Pacific coral reefs: effects of reef habitat, depth, and wave energy gradients on spatial patterns. PeerJ 1, e81. doi:10.7717/peerj.81.

Willmott, C., 1982. Some comments on the evaluation of model performance. Bull. Am. Meteorol. Soc. doi:10.1175/1520-0477(1982)063⟨1309:SCOTEO⟩2.0.CO;2.

Wolanski, E., Asaeda, T., Tanaka, A., Deleersnijder, E., 1996. Three-dimensional island wakes in the field, laboratory experiments and numerical models. Cont. Shelf Res. 16, 1437–1452.

Yahel, G., Post, A.F., Fabricius, K., Marie, D., Vaulot, D., Genin, A., 1998. Phytoplankton distribution and grazing near coral reefs. Limnol. Oceanogr. 43, 551–563.

Young, I.R., 1989. Wave transformation over coral reefs. J. Geophys. Res. 94, 9779. doi:10.1029/JC094iC07p09779.